

Spectrum Dependent Learning Curves in Kernel Regression and Wide Neural Networks

Blake Bordelon¹ Abdulkadir Canatar² Cengiz Pehlevan^{1,3}

Abstract

A fundamental question in modern machine learning is how deep neural networks can generalize. We address this question using 1) an equivalence between training infinitely wide neural networks and performing kernel regression with a deterministic kernel called the Neural Tangent Kernel (NTK) (Jacot et al., 2018), and 2) theoretical tools from Gaussian processes and statistical physics. We derive analytical expressions for learning curves for kernel regression, and use them to evaluate how the test loss of a trained neural network depends on the number of samples. Our approach allows us not only to compute the total test risk but also the decomposition of the risk due to different spectral components of the kernel. Complementary to recent results showing that during gradient descent, neural networks fit low frequency components first, we identify a new type of frequency principle: as the size of the training set size grows, kernel machines and neural networks begin to fit successively higher frequency modes of the target function. We verify our theory with simulations of kernel regression and training wide artificial neural networks.

1. Introduction

Deep learning has reached unparalleled performance in a variety of tasks and revolutionized many fields (LeCun et al., 2015), yet there are many important theoretical questions about it that are unanswered. Perhaps the most important one is the question of generalization: how a deep network can predict accurately on data that it has not seen before. In this paper, we present a theory of generalization in kernel machines and wide neural networks. We ask how gener-

alization performance depends on the number of training examples a network sees, a notion captured by learning curves. Such performance is expected to also depend on other factors such as the network’s architecture and the complexity of the learning task, yet identifying precisely how these factors impact generalization poses a theoretical challenge.

In order to address these questions, we work in a limit of neural networks where training dynamics simplifies. When the hidden layers of a neural network are taken to infinite width with a certain initialization scheme, recent influential work (Jacot et al., 2018; Arora et al., 2019; Lee et al., 2019) showed that training a feedforward neural network with gradient descent to zero training loss is equivalent to kernel interpolation (or ridgeless kernel regression) with a kernel called the Neural Tangent Kernel (NTK) (Jacot et al., 2018). Exploiting this correspondence, we develop an approximate theory of generalization in kernel regression and use our findings to get insight into deep neural networks in the NTK limit. Our kernel regression theory is generally applicable to any kernel and contains kernel interpolation as a special limit (ridge parameter going to zero).

The goal of our theory is not to provide worst case bounds on generalization performance in the sense of statistical learning theory (Vapnik, 1999), but to provide analytical expressions that explain the average or a typical performance, in the spirit of statistical physics. The techniques we use are a continuous approximation to learning curves previously used in Gaussian processes (Sollich, 1999; 2002; Sollich & Halees, 2002) and the replica trick of statistical physics (Sherrington & Kirkpatrick, 1975; Mézard et al., 1987).

Our contributions and results are summarized below:

- Using a continuous approximation to learning curves adapted from Gaussian process literature (Sollich, 1999; 2002), we derive analytical expressions for learning curves for each spectral component of a target function learned through kernel regression.
- We present another way to arrive at the same analytical expressions using the replica trick of statistical physics and a saddle-point approximation (Sherrington & Kirkpatrick, 1975; Mézard et al., 1987).
- Analysis of our theoretical expressions show that differ-

¹John A. Paulson School of Engineering and Applied Sciences, Harvard University, Cambridge, MA, USA ²Physics Department, Harvard University, Cambridge, MA, USA ³Center for Brain Science, Harvard University, Cambridge, MA, USA. Correspondence to: Cengiz Pehlevan <cpehlevan@seas.harvard.edu>.

ent spectral modes of a target function are learned with different rates. Modes corresponding to higher kernel eigenvalues are learned faster, in the sense that a marginal training data point causes a greater percent change in generalization error for high eigenvalue modes than for low eigenvalue modes.

- When data is sampled from a uniform distribution on a hypersphere, dot product kernels, which include NTK, admit a degenerate Mercer decomposition in spherical harmonics, Y_{km} . In this case, our theory predicts that generalization error of lower frequency modes of the target function decrease more quickly than higher frequency modes as the dataset size grows. Different learning stages are visible in the sense described below.
- As the dimensions of data, d , go to infinity, learning curves exhibit different learning stages. For a training set of size $p \sim \mathcal{O}(d^l)$, modes with $k < l$ are perfectly learned, $k = l$ are being learned, and $k > l$ are not learned.
- We verify the predictions of our theory using numerical simulations for kernel regression and kernel interpolation with NTK, and wide and deep neural networks trained with gradient descent. Our theory fits experiments remarkably well.

1.1. Related Work

Our main approximation technique comes from the literature on Gaussian processes, which is related to kernel regression in a certain limit. Total learning curves, but not their spectral decomposition as we do here, for Gaussian processes have been studied in a limited teacher-student setting where both student and teacher were described by the same Gaussian process and the same noise in (Oppor & Vivarelli, 1999; Sollich, 1999). Here we allow any teacher distribution including a single fixed teacher. Sollich also considered mismatched models where teacher and student kernels had different eigenspectra and different noise levels (Sollich, 2002). The total learning curve from this model is consistent with our results when the teacher noise sent to zero, but we also consider, provide and analyze generalization in spectral modes. We use an analogue of the “lower-continuous” approximation scheme introduced in (Sollich & Halees, 2002), which we also reproduce here through a replica trick and saddle-point approximation.

Generalization bounds for kernel ridge regression have been obtained in many contexts (Scholkopf & Smola, 2001; Cucker & Smale, 2002; Vapnik, 1999; Györfi et al., 2003), but the rates of convergence often crucially depend on the explicit ridge parameter λ and do not provide guarantees in the ridgeless case. Recently, interest in explaining the phenomenon of interpolation has led to the study of ridgeless regression (Belkin et al., 2018c;b; 2019; Liang & Rakhlin, 2018), where generalization bounds are kernel and data de-

pendent. In this work, our aim is to capture the average case performance of kernel regression in a spectrum dependent model that remains valid in the ridgeless case.

In statistical physics domain, (Dietrich et al., 1999) calculated learning curves for support vector machines, but not kernel regression, in the limit of number of training samples going to infinity for dot product kernels with binary inputs using a replica method. Our theory applies to general kernels and finite size datasets. In the infinite training set limit, they observed several learning stages where each spectral modes are learned with different rates. We observe similar phenomena in kernel regression as summarized above. In a similar spirit, (Cohen et al., 2019) calculates learning curves for infinite-width neural networks using a path integral formulation and a replica analysis but do not discuss the spectral dependence of the test risk as we do here.

In the infinite width limit we are considering, neural networks have many more parameters than training samples. Some works have explained generalization of overparameterized neural networks as a consequence of the training procedure since stochastic gradient descent exhibits an implicit bias towards choosing the simplest functions that interpolate the training data (Belkin et al., 2018a;c; Luo et al., 2019; Jacot et al., 2018). Empirical studies have shown that neural networks fit the low frequency components of the target before the high frequency components during training with gradient descent (Rahaman et al., 2018). In addition to training dynamics, recent works such as (Yang & Salman, 2019; Bietti & Mairal, 2019; Cao et al., 2019) have discussed how the spectrum of kernels impacts its smoothness and approximation properties. Here we explore similar ideas by explicitly calculating average case learning curves for kernel regression and studying its dependence on the kernel’s eigenspectrum.

2. Kernel Regression Learning Curves

We start with a general theory of kernel regression. Implications of our theory for dot product kernels including NTK, and its relation to trained neural networks are described in Section 3.

2.1. Notation and Problem Setup

We start by defining our notation and setting up our problem. Our initial goal is to derive a mathematical expression for generalization error in kernel regression, which we will analyze in the subsequent sections using techniques from the Gaussian process literature (Sollich, 1999; 2002; Sollich & Halees, 2002) and statistical physics (Sherrington & Kirkpatrick, 1975; Mézard et al., 1987).

The goal of kernel regression is to learn a function $f : \mathcal{X} \rightarrow \mathbb{R}$ from a finite number of observations (Wahba, 1990;

Scholkopf & Smola, 2001). Let $\{\mathbf{x}_i, y_i\} \in \mathcal{X} \times \mathbb{R}$, where $\mathcal{X} \subseteq \mathbb{R}^d$, be one of the p training examples and let \mathcal{H} be a Reproducing Kernel Hilbert space (RKHS) with inner product $\langle \cdot, \cdot \rangle_{\mathcal{H}}$. Kernel ridge regression is defined as:

$$\min_{f \in \mathcal{H}} \sum_{i=1}^p (f(\mathbf{x}_i) - y_i)^2 + \lambda \|f\|_{\mathcal{H}}^2. \quad (1)$$

$\lambda \rightarrow 0$ limit is referred to as interpolating kernel regression, and, as we will discuss later, relevant to training wide neural networks. The unique minimum of the convex kernel regression loss is given by

$$f(\mathbf{x}) = \mathbf{y}^\top (\mathbf{K} + \lambda \mathbf{I})^{-1} \mathbf{k}(\mathbf{x}), \quad (2)$$

where $K(\cdot, \cdot)$ is the reproducing kernel for \mathcal{H} , \mathbf{K} is the $p \times p$ kernel gram matrix $K_{ij} = K(\mathbf{x}_i, \mathbf{x}_j)$, and $k(\mathbf{x})_i = K(\mathbf{x}, \mathbf{x}_i)$. Lastly, $\mathbf{y} \in \mathbb{R}^p$ is the vector of target values $y_i = f^*(\mathbf{x}_i)$. For interpolating kernel regression, the solution is the same except that $\lambda = 0$, meaning that training data is fit perfectly. The proof of this optimal solution is provided in the Supplementary Information (SI) Section 1.

Let $p(\mathbf{x})$ be the probability density function from which the input data are sampled. The generalization error is defined as the expected risk with expectation taken over new test points sampled from the same density $p(\mathbf{x})$. For a given dataset $\{\mathbf{x}_i\}$ and target function $f^*(\mathbf{x})$, let $f_K(\mathbf{x}; \{\mathbf{x}_i\}, f^*)$ represent the function learned with kernel regression. The generalization error for this dataset and target function is

$$E_g(\{\mathbf{x}_i\}, f^*) = \int d\mathbf{x} p(\mathbf{x}) (f_K(\mathbf{x}; \{\mathbf{x}_i\}, f^*) - f^*(\mathbf{x}))^2. \quad (3)$$

To calculate the *average case* performance of kernel regression, we average this generalization error over the possible datasets $\{\mathbf{x}_i\}$ and teacher functions f^*

$$E_g = \langle E_g(\{\mathbf{x}_i\}, f^*) \rangle_{\{\mathbf{x}_i\}, f^*}. \quad (4)$$

Our aim is to calculate E_g for a general kernel, and distribution over teacher functions.

For our theory, we will find it convenient to work with the feature map defined by the Mercer decomposition. By Mercer's theorem (Mercer, 1909; Rasmussen & Williams, 2005), the kernel admits a representation in terms of its M kernel eigenfunctions $\{\phi_\rho(\mathbf{x})\}$,

$$K(\mathbf{x}, \mathbf{x}') = \sum_{\rho=1}^M \lambda_\rho \phi_\rho(\mathbf{x}) \phi_\rho(\mathbf{x}') = \sum_{\rho=1}^M \psi_\rho(\mathbf{x}) \psi_\rho(\mathbf{x}_i), \quad (5)$$

where $\psi_\rho(\mathbf{x}) = \sqrt{\lambda_\rho} \phi_\rho(\mathbf{x})$ is the feature map we will work with. In our analysis, M will be taken to be infinite, but for the development of the learning curves, we will first consider M as a finite integer. The eigenfunctions and eigenvalues

are defined with respect to the probability measure that generates the data $d\mu(\mathbf{x}) = p(\mathbf{x})d\mathbf{x}$

$$\int d\mathbf{x}' p(\mathbf{x}') K(\mathbf{x}, \mathbf{x}') \phi_\rho(\mathbf{x}') = \lambda_\rho \phi_\rho(\mathbf{x}). \quad (6)$$

We will also find it convenient to work with a vector representation of the RKHS functions in the feature space. To do so, we note that the kernel eigenfunctions form a complete orthonormal basis for square integrable functions $L_2(\mathcal{X})$ as $M \rightarrow \infty$, allowing the expansion of the target function f^* and learned function f in terms of features $\{\psi_\rho(\mathbf{x})\}$

$$f^*(\mathbf{x}) = \sum_{\rho} \bar{w}_\rho \psi_\rho(\mathbf{x}), \quad f(\mathbf{x}) = \sum_{\rho} w_\rho \psi_\rho(\mathbf{x}). \quad (7)$$

Hence, M -dimensional vectors \mathbf{w} and $\bar{\mathbf{w}}$ constitute a representation of f and f^* respectively in the feature space.

We can also obtain a feature space expression for the optimal kernel regression function (2). Let $\Psi \in \mathbb{R}^{M \times p}$ be feature matrix for the sample so that $\Psi_{\rho,i} = \psi_\rho(\mathbf{x}_i)$. With this representation, kernel ridge regression (1) can be recast as the optimization problem $\min_{\mathbf{w} \in \mathbb{R}^M, \|\mathbf{w}\|_2 < \infty} \|\Psi^\top \mathbf{w} - \mathbf{y}\|^2 + \lambda \|\mathbf{w}\|^2$, whose solution is

$$\mathbf{w} = (\Psi \Psi^\top + \lambda \mathbf{I})^{-1} \Psi \mathbf{y}. \quad (8)$$

Another novelty of our theory is the decomposition of the test risk into its contributions from different eigenmodes. The feature space expression of the generalization error after averaging over the test distribution can be written as:

$$E_g = \sum_{\rho} E_\rho, \quad E_\rho \equiv \lambda_\rho \langle (w_\rho - \bar{w}_\rho)^2 \rangle_{\{\mathbf{x}_i\}, \bar{\mathbf{w}}}, \quad (9)$$

where we identify E_ρ as the generalization error in mode ρ .

Proof.

$$\begin{aligned} E_g &= \langle (f(\mathbf{x}) - f^*(\mathbf{x}))^2 \rangle_{\mathbf{x}, \{\mathbf{x}_i\}, f^*} \\ &= \sum_{\rho, \gamma} \langle (w_\rho - \bar{w}_\rho)(w_\gamma - \bar{w}_\gamma) \rangle_{\{\mathbf{x}_i\}, f^*} \langle \psi_\rho(\mathbf{x}) \psi_\gamma(\mathbf{x}) \rangle_{\mathbf{x}} \\ &= \sum_{\rho} \lambda_\rho \langle (w_\rho - \bar{w}_\rho)^2 \rangle_{\{\mathbf{x}_i\}, \bar{\mathbf{w}}} = \sum_{\rho} E_\rho. \end{aligned} \quad (10)$$

□

Finally, with our notation set up, we can present our first result about generalization error.

Proposition 1. *For the \mathbf{w} that minimizes the training error, if the training examples are produced by a target function $\mathbf{y} = \Psi^\top \bar{\mathbf{w}}$, we find that the generalization error is given by*

$$E_g = \text{Tr} \left(\mathbf{D} \langle \mathbf{G}^2 \rangle_{\{\mathbf{x}_i\}} \right), \quad (11)$$

which can be decomposed into modal generalization errors

$$E_\rho = \sum_{\gamma} \mathbf{D}_{\rho,\gamma} \langle \mathbf{G}_{\gamma,\rho}^2 \rangle_{\{\mathbf{x}_i\}}, \quad (12)$$

where

$$\mathbf{G} = \left(\frac{1}{\lambda} \Phi \Phi^\top + \Lambda^{-1} \right)^{-1}, \quad \Phi = \Lambda^{-1/2} \Psi. \quad (13)$$

and

$$\mathbf{D} = \Lambda^{-1/2} \langle \overline{\mathbf{w}\mathbf{w}^\top} \rangle_{\overline{\mathbf{w}}} \Lambda^{-1/2}. \quad (14)$$

We leave the proof to SI Section 2 but provide a few cursory observations of this result. First, note that all of the dependence on the teacher function comes in the matrix \mathbf{D} whereas all of the dependence on the empirical samples is in \mathbf{G} . In the rest of the paper, we will develop multiple theoretical methods to calculate the generalization error given by expression (11).

Averaging over the target weights in the expression for \mathbf{D} is easily done for generic weight distributions. The case of a fixed target is included by choosing a delta-function distribution over $\overline{\mathbf{w}}$.

We present two methods for computing the nontrivial average of the matrix \mathbf{G}^2 over the training samples $\{\mathbf{x}_i\}$. First, we consider the effect of adding a single new sample to \mathbf{G} to derive a recurrence relation for \mathbf{G} at different number of data points. This method generates a partial differential equation that must be solved to compute the generalization error. Second, we use a replica method and a saddle point approximation to calculate the generalization error by computing the average log-determinant of \mathbf{G}^{-1} . These approaches give identical predictions for the learning curves of kernel machines.

For notational simplicity, in the rest of the paper, we will use $\langle \dots \rangle$ to mean $\langle \dots \rangle_{\{\mathbf{x}_i\}, \overline{\mathbf{w}}}$ unless stated otherwise. In all cases, the quantity inside the brackets will depend either on the data distribution or the distribution of target weights, but not both.

2.2. Continuous Approximation to Learning Curves

First, we adapt a method following Sollich (Sollich, 1999; 2002; Sollich & Halees, 2002), to calculate the generalization error. We generalize the definition of \mathbf{G} by introducing an auxiliary parameter v , and make explicit its dataset size, p , dependence:

$$\tilde{\mathbf{G}}(p, v) = \left(\frac{1}{\lambda} \Phi \Phi^\top + \Lambda^{-1} + v \mathbf{I} \right)^{-1}. \quad (15)$$

Note that the quantity we want to calculate is given by

$$\langle \mathbf{G}^2(p) \rangle = - \frac{\partial}{\partial v} \langle \tilde{\mathbf{G}}(p, v) \rangle \Big|_{v=0}. \quad (16)$$

By considering the effect of adding a single randomly sampled input \mathbf{x}' , and treating p as a continuous parameter, we can derive an approximate quasi-linear partial differential equation (PDE) for the average elements of \mathbf{G} as a function of the number of data points p (see below for a derivation):

$$\frac{\partial \langle \tilde{\mathbf{G}}(p, v) \rangle}{\partial p} = \frac{1}{\lambda + \text{Tr} \langle \tilde{\mathbf{G}}(p, v) \rangle} \frac{\partial}{\partial v} \langle \tilde{\mathbf{G}}(p, v) \rangle, \quad (17)$$

with the initial condition $\tilde{\mathbf{G}}(0, v) = (\Lambda^{-1} + v \mathbf{I})^{-1}$, which follows from $\Phi \Phi^\top = 0$ when there is no data. Since $\tilde{\mathbf{G}}$ is initialized as a diagonal matrix, the off-diagonal elements will not vary under the dynamics and $\langle \tilde{\mathbf{G}}(p, v) \rangle$ will remain diagonal for all (p, v) . We will use the solutions to this PDE and relation (16) to arrive at an approximate expression for the generalization error E_g and the mode errors E_ρ .

Derivation of the PDE approximation (17). Let $\phi \in \mathbb{R}^M$ represent the new feature to be added to \mathbf{G}^{-1} so that $\phi_\rho = \phi_\rho(\mathbf{x}')$ where $\mathbf{x}' \sim p(\mathbf{x}')$ is a random sample from the data distribution. Let $\langle \tilde{\mathbf{G}}(p, v) \rangle_\Phi$ denote the matrix $\tilde{\mathbf{G}}$ averaged over its p -sample design matrix Φ . By the Woodbury matrix inversion formula

$$\begin{aligned} \langle \tilde{\mathbf{G}}(p+1, v) \rangle_{\Phi, \phi} &= \left\langle \left(\tilde{\mathbf{G}}(p, v)^{-1} + \frac{1}{\lambda} \phi \phi^\top \right)^{-1} \right\rangle_{\Phi, \phi} \\ &= \langle \tilde{\mathbf{G}}(p, v) \rangle_\Phi - \left\langle \frac{\tilde{\mathbf{G}}(p, v) \phi \phi^\top \tilde{\mathbf{G}}(p, v)}{\lambda + \phi^\top \tilde{\mathbf{G}}(p, v) \phi} \right\rangle_{\Phi, \phi}. \end{aligned} \quad (18)$$

Performing the average of the last term on the right hand side is difficult so we resort to an approximation, where the numerator and denominator are averaged separately.

$$\langle \tilde{\mathbf{G}}(p+1, v) \rangle_{\Phi, \phi} \approx \langle \tilde{\mathbf{G}}(p, v) \rangle_\Phi - \frac{\langle \tilde{\mathbf{G}}(p, v)^2 \rangle_\Phi}{\lambda + \text{Tr} \langle \tilde{\mathbf{G}}(p, v) \rangle_\Phi}, \quad (19)$$

where we used the fact that $\langle \phi_\rho(\mathbf{x}') \phi_\gamma(\mathbf{x}') \rangle_{\mathbf{x}' \sim p(\mathbf{x}')} = \delta_{\rho, \gamma}$.

Treating p as a continuous variable and taking a continuum limit of the finite differences given above, we arrive at (17). \square

Next, we present the solution to the PDE (17).

Proposition 2. Let $g_\rho(p, v) = \langle \tilde{\mathbf{G}}(p, v)_{\rho\rho} \rangle$ represent the diagonal elements of the average matrix $\langle \tilde{\mathbf{G}}(p, v) \rangle$. These matrix elements satisfy the implicit relationship

$$g_\rho(p, v) = \left(\frac{1}{\lambda_\rho} + v + \frac{p}{\lambda + \sum_{\gamma=1}^M g_\gamma(p, v)} \right)^{-1}. \quad (20)$$

This implicit solution is obtained from the method of characteristics which we provide in Section 3 of the SI. The proof relies on the observation that each of the matrix elements depend explicitly on p, v and the trace $t(p, v) = \sum_{\rho} g_{\rho}(p, v)$. Once $t(p, v)$ is solved for, the result above is immediate.

Proposition 3. *Under the PDE approximation (17), the average error E_{ρ} associated with mode ρ is*

$$E_{\rho}(p) = \frac{\langle \bar{w}_{\rho}^2 \rangle}{\lambda_{\rho}} \left(\frac{1}{\lambda_{\rho}} + \frac{p}{\lambda + t(p)} \right)^{-2} \left(1 - \frac{p\gamma(p)}{(\lambda + t(p))^2} \right)^{-1}, \quad (21)$$

where $t(p)$ is the solution to the implicit equation

$$t(p) = \sum_{\rho} \left(\frac{1}{\lambda_{\rho}} + \frac{p}{\lambda + t(p)} \right)^{-1}, \quad (22)$$

and $\gamma(p)$ is defined as

$$\gamma(p) = \sum_{\rho} \left(\frac{1}{\lambda_{\rho}} + \frac{p}{\lambda + t(p)} \right)^{-2}. \quad (23)$$

The full proof of this proposition is provided in Section 3 of the SI. We show the steps required to compute theoretical learning curves numerically in Algorithm 1.

In these expressions, the target function sets the overall scale of E_{ρ} . The spectrum of the kernel affects all modes in a non-trivial way. When we apply this theory to neural networks in Section (3), the information about the architecture of the network will be in the spectrum $\{\lambda_{\rho}\}$. The dependence on number of samples p is also nontrivial, but we will consider various informative limits below.

Next, we consider another theoretical method to obtain the same learning curves for kernel regression.

2.3. Replica Trick and Finite- p Saddle-Point Approximation

The result of the continuous approximation can be obtained using another approximation method, which we outline here and detail in SI Section 4. We perform the average of matrix \mathbf{G}^2 over the training data, using the replica trick (Sherrington & Kirkpatrick, 1975; Mézard et al., 1987) from statistical physics and a finite size saddle-point approximation, which yields identical learning curves to Proposition 3.

The calculation proceeds by recasting the generalization error in terms of the log determinant of \mathbf{G}^{-1} . First, we generalize the definition of \mathbf{G} once again

$$\tilde{\mathbf{G}} = \left(\frac{1}{\lambda} \Phi \Phi^{\top} + \Lambda^{-1} + v\mathbf{I} + \chi \mathbf{D} \right)^{-1}. \quad (24)$$

With this definition, the generalization error for a fixed

Algorithm 1 Computing Theoretical Learning Curves

Input: RKHS spectrum $\{\lambda_{\rho}\}$, target function weights $\{\bar{w}_{\rho}\}$, regularizer λ , sample sizes $\{p_i\}$, $i = 1, \dots, m$;
for $i = 1$ **to** m **do**

Solve numerically $t_i = \sum_{\rho} \left(\frac{1}{\lambda_{\rho}} + \frac{p_i}{\lambda + t_i} \right)^{-1}$

Compute $\gamma_i = \sum_{\rho} \left(\frac{1}{\lambda_{\rho}} + \frac{p_i}{\lambda + t_i} \right)^{-2}$

$E_{\rho,i} = \frac{\langle \bar{w}_{\rho}^2 \rangle}{\lambda_{\rho}} \left(\frac{1}{\lambda_{\rho}} + \frac{p_i}{\lambda + t_i} \right)^{-2} \left(1 - \frac{p_i \gamma_i}{(\lambda + t_i)^2} \right)^{-1}$

end for

teacher is given by

$$E_g = 2 \frac{\partial^2}{\partial \chi \partial v} \left\langle \log \det \tilde{\mathbf{G}}^{1/2} \right\rangle \Big|_{v=0, \chi=0}. \quad (25)$$

We identify the partition function and represent it with a Gaussian integral

$$Z = \det \tilde{\mathbf{G}}^{1/2} = \int \frac{d\mathbf{u}}{\sqrt{(2\pi)^M}} e^{-\frac{1}{2} \mathbf{u}^{\top} \tilde{\mathbf{G}}^{-1} \mathbf{u}}. \quad (26)$$

As before, the difficulty in the calculation is averaging over the training samples: *i.e.* performing $\langle \log Z \rangle$. To analytically perform this average, we resort to the replica method to compute the free energy $\langle \log Z \rangle = \lim_{n \rightarrow 0} \frac{\partial}{\partial n} \log \langle Z^n \rangle$ by computing integer moments of Z .

The calculation is detailed in SI Section 4 and mostly follows the well-known steps. We approximate the integral that results from performing the data average of $\langle Z^n \rangle$ with a saddle-point approximation under a decoupled replica symmetric ansatz and arrive at the same result for learning curves as acquired from the continuous approximation, Proposition 3. We note that to develop a theory for learning curves for finite sample sizes, we evaluated the saddle point at a finite p . This is different than the usual application of the replica method where a thermodynamic limit ($p \rightarrow \infty$) is taken (Mézard et al., 1987). In another work, we will provide a detailed account of the $p \rightarrow \infty$ replica theory for this problem.

2.4. Spectral Dependency of Learning Curves

We can get insight about the behavior of learning curves by considering ratios between errors in different modes:

$$\frac{E_{\rho}}{E_{\gamma}} = \frac{\langle \bar{w}_{\rho}^2 \rangle}{\langle \bar{w}_{\gamma}^2 \rangle} \frac{\lambda_{\gamma}}{\lambda_{\rho}} \frac{\left(\frac{1}{\lambda_{\gamma}} + \frac{p}{\lambda + t} \right)^2}{\left(\frac{1}{\lambda_{\rho}} + \frac{p}{\lambda + t} \right)^2}. \quad (27)$$

For small p this ratio approaches $\frac{E_{\rho}}{E_{\gamma}} \sim \frac{\lambda_{\rho} \langle \bar{w}_{\rho}^2 \rangle}{\lambda_{\gamma} \langle \bar{w}_{\gamma}^2 \rangle}$. For large p , $\frac{E_{\rho}}{E_{\gamma}} \sim \frac{\langle \bar{w}_{\rho}^2 \rangle / \lambda_{\rho}}{\langle \bar{w}_{\gamma}^2 \rangle / \lambda_{\gamma}}$, indicating that asymptotically ($p \rightarrow \infty$), the amount of error in mode ρ grows with the ratio $\langle \bar{w}_{\rho}^2 \rangle / \lambda_{\rho}$,

showing that the asymptotic mode error is large if the teacher function places large amounts of power in modes that have small RKHS eigenvalues λ_ρ .

We can also examine how the RKHS spectrum affects the evolution of the error ratios with p . Without loss of generality, we take $\lambda_\gamma > \lambda_\rho$ and note that

$$\frac{1}{2} \frac{d}{dp} \log \left(\frac{E_\rho}{E_\gamma} \right) = \left[\frac{1}{\frac{1}{\lambda_\rho} + \frac{p}{\lambda+t}} - \frac{1}{\frac{1}{\lambda_\gamma} + \frac{p}{\lambda+t}} \right] \frac{1}{\gamma} \frac{\partial t}{\partial p}. \quad (28)$$

Since $\lambda_\gamma > \lambda_\rho$ and $\frac{\partial t}{\partial p} = -\frac{1}{\lambda+t} \text{Tr}(\mathbf{G}^2) < 0$ (SI Section 9), we have $\frac{d}{dp} \log E_\rho > \frac{d}{dp} \log E_\gamma$. In this sense, the marginal training data point causes a greater percent change in generalization error for modes with larger RKHS eigenvalues.

3. Dot Product Kernels on \mathbb{S}^{d-1} and NTK

For the remainder of the paper, we specialize to the case where our inputs are drawn uniformly on $\mathcal{X} = \mathbb{S}^{d-1}$, a $(d-1)$ -dimensional unit hyper-sphere. In addition, we will assume that the kernel is a dot product kernel ($K(\mathbf{x}, \mathbf{x}') = \kappa(\mathbf{x}^\top \mathbf{x}')$), as is the case for NTK. In this setting, the kernel eigenfunctions are spherical harmonics $\{Y_{km}\}$ (Bietti & Mairal, 2019; Efthimiou & Frye, 2014), and the Mercer decomposition is given by

$$K(\mathbf{x}, \mathbf{x}') = \sum_{k=0}^{\infty} \lambda_k \sum_{m=1}^{N(d,k)} Y_{km}(\mathbf{x}) Y_{km}(\mathbf{x}'). \quad (29)$$

Here, $N(d, k)$ is the dimension of the subspace spanned by d -dimensional spherical harmonics of degree k . Rotation invariance renders the eigenspectrum degenerate since each of the $N(d, k)$ modes of frequency k share the same eigenvalue λ_k . A review of these topics is given in SI Sections 5 and 6.

We briefly comment on another fact that will be used in our numerical simulations. Dot product kernels admit an expansion in terms of Gegenbauer polynomials $\{Q_k\}$, which form a complete and orthonormal basis for the uniform measure on the sphere (Dai & Xu, 2013). The Gegenbauer polynomials can be further expanded in terms of spherical harmonics $\{Y_{km}\}$ (Dai & Xu, 2013) (see SI Sections 5 and 6 for a review). This yields an alternative derivation of (29): $K(\mathbf{x}, \mathbf{x}') = \sum_{k=0}^{\infty} \lambda_k N(d, k) Q_k(\mathbf{x}^\top \mathbf{x}') = \sum_{k=0}^{\infty} \lambda_k \sum_{m=1}^{N(d,k)} Y_{km}(\mathbf{x}) Y_{km}(\mathbf{x}')$.

3.1. Frequency Dependency of Learning Curves

In the special case of dot product kernels with monotonically decaying spectra, the result given in equation (28) indicates that the marginal training data point causes greater reduction in relative error for low frequency modes than

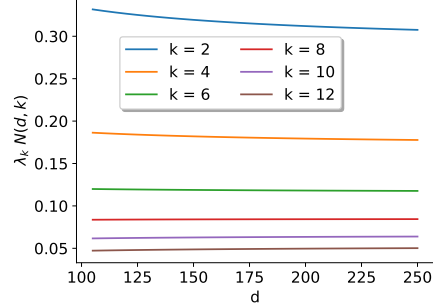


Figure 1. Spectrum of 10-layer NTK multiplied by degeneracy as a function of dimension for various k , calculated by numerical integration (SI Section 6). $\lambda_k N(d, k)$ stays constant as input dimension increases, confirming that $\lambda_k N(d, k)^{-1} \sim \mathcal{O}(1)$ at large d .

for high frequency modes. This exercise illustrates that monotonic RKHS spectra represent an inductive bias that preferentially favors fitting lower frequencies as more data becomes available. More rapid decay in the spectrum yields a stronger bias to fit low frequencies first.

To make this intuition more precise, we now discuss an informative limit $d \rightarrow \infty$ where the degeneracy factor approaches $N(d, k) \sim d^k$. In the following, we replace eigenfunction index ρ with index pair (k, m) . Eigenvalues of the kernel scales with d as $\lambda_k \sim N(d, k)^{-1}$ (Smola et al., 2001) in the $d \rightarrow \infty$ limit, as we verify numerically in Figure 1 for NTK. If we take $p = \alpha d^\ell$ for some integer degree ℓ , then E_{km} exhibits three distinct learning stages. Leaving the details to SI Section 10, we find that in this limit, for large α :

$$\frac{E_{km}(\alpha)}{E_{km}(0)} = \begin{cases} 1, & k > \ell \\ \frac{\text{const.}}{\alpha^2}, & k = \ell \\ 0, & k < \ell \end{cases}, \quad (30)$$

where the constant is given in Section 10. In other words, $k < \ell$ modes are perfectly learned, $k = \ell$ are being learned with an asymptotic $1/\alpha^2$ rate, and $k > \ell$ are not learned.

This simple calculation demonstrates that the lower modes are learned earlier with increasing sample complexity since the higher modes stays stationary until p reaches to the degeneracy of that mode.

3.2. Neural Tangent Kernel and its Spectrum

The NTK is a rotation invariant kernel that describes how the predictions of infinitely wide neural networks evolve under gradient flow (Jacot et al., 2018). Let θ_i index all of the parameters of the neural network and let $f_\theta(\mathbf{x})$ be the output of the network. Here, we focus on scalar network outputs for simplicity. Then the neural tangent kernel is

defined as

$$K_{\text{NTK}}(\mathbf{x}, \mathbf{x}') = \sum_i \left\langle \frac{\partial f_\theta(\mathbf{x})}{\partial \theta_i} \frac{\partial f_\theta(\mathbf{x}')}{\partial \theta_i} \right\rangle_\theta. \quad (31)$$

Let $\mathbf{u}_\theta \in \mathbb{R}^p$ be the current predictions of f_θ on the training data. If the parameters of the model are updated via gradient flow, $\frac{d\theta}{dt} = -\nabla_\theta \mathbf{u}_\theta \cdot (\mathbf{u}_\theta - \mathbf{y})$, then the predictions on the training data evolve with the dynamics

$$\frac{d\mathbf{u}_\theta}{dt} = -\mathbf{K}_{\text{NTK}} \cdot (\mathbf{u}_\theta - \mathbf{y}). \quad (32)$$

When the width of the neural network is taken to infinity with proper initialization (where the weights at layer ℓ are sampled $W^{(\ell)} \sim \mathcal{N}(0, \frac{1}{n^{(\ell)}})$ where $n^{(\ell)}$ is the number of hidden units in layer ℓ) the NTK becomes independent of the particular realization of parameters and approaches to a deterministic function of the inputs and the nonlinear activation function (Jacot et al., 2018). Further, the kernel is approximately fixed throughout gradient descent (Jacot et al., 2018; Arora et al., 2019). If we assume that $\mathbf{u}_\theta = 0$ at $t = 0$, then the final learned function is

$$f(\mathbf{x}) = \mathbf{y}^\top \mathbf{K}_{\text{NTK}}^{-1} \mathbf{k}(\mathbf{x}). \quad (33)$$

Note that this corresponds to ridgeless, interpolating regression where $\lambda = 0$. We will use this correspondence and our kernel regression theory to explain neural network learning curves in the next section. For more information about NTK for fully connected architectures see Section 7 and 8 of the SI.

To generate theoretical learning curves, we need the eigen-spectrum of the kernels involved. As a dot product kernel, since NTK lives on \mathbb{S}^{d-1} , it suffices to calculate the inner products $\langle K_{\text{NTK}}(\mathbf{x}), Q_k(\mathbf{x}) \rangle$ over \mathbb{S}^{d-1} , which we evaluate numerically with Gauss-Gegenbauer quadrature (SI Section 6). The NTK spectrum $\lambda_k N(d, k)$ is shown as a function of input dimension (Figure 1), which verifies that for large dimensions, NTK spectrum stays constant as the dimension increases.

4. Experiments

In this section, we test our theoretical results for kernel regression, kernel interpolation and wide networks.

4.1. Kernel Regression and Interpolation

We first test our theory in a kernel regression task. In this experiment, the target function is a linear combination of a kernel evaluated at randomly sampled points $\{\bar{\mathbf{x}}_i\}$:

$$f^*(\mathbf{x}) = \sum_{i=1}^{p'} \bar{\alpha}_i K(\mathbf{x}, \bar{\mathbf{x}}_i), \quad (34)$$

where $\bar{\alpha}_i \sim \mathcal{B}(1/2)$ are sampled randomly from a Bernoulli distribution on $\{\pm 1\}$ and $\bar{\mathbf{x}}_i$ are sampled uniformly from \mathbb{S}^{d-1} . The points $\bar{\mathbf{x}}_i$ are independent samples from \mathbb{S}^{d-1} and are different than the training set $\{\mathbf{x}_i\}$. The student function is learned with kernel regression by inverting the gram matrix \mathbf{K} defined on the training samples $\{\mathbf{x}_i\}$ according to equation (2). With this choice of target function, exact computation of the mode wise errors $E_k = \sum_m E_{km}$ in terms of Gegenbauer polynomials is possible; the formula and its derivation are provided in section 11.2 of the SI. We compare these experimental mode-errors to those predicted by our theory and find perfect agreement. For these experiments, both the target and student kernels are taken to be NTK of a 4 layer fully connected ReLU without bias. Figure 2 shows the errors for each frequency k as a function of sample size p . In accordance with our theory, higher frequency modes require more data to fit.

The different panels of Figure 2 shows the effect of regularization and increased input dimension. In Figure 2(a), we show the mode errors for ridge regression with an explicit regularization penalty ($\lambda = 5$, $d = 10$) while Figure 2(b) shows the learning curves for ridgeless regression ($\lambda = 0$, $d = 10$). In both figures $p' = 300$. The higher ridge parameter causes the learning curves to be learned more slowly. Figure 2(c) shows the effect of increasing the input dimension to $d = 100$. Consistent with our theory, higher input dimension causes the higher frequency modes to be learned at much larger p .

4.2. Learning Curves for Finite Width Neural Networks

Having established that our theory accurately predicts the generalization error of kernel regression with the NTK, we now compare the generalization error of finite width neural networks with the theoretical learning curves for NTK. For these experiments, we use the neural-tangents library (Novak et al., 2020) which supports training and inference for both finite and infinite width neural networks.

First, we use ‘‘pure mode’’ teacher functions, meaning the teacher is composed only of spherical harmonics of the same degree. For ‘‘pure mode’’ k , the teacher is constructed with the following rule:

$$f^*(\mathbf{x}) = \sum_{i=1}^{p'} \bar{\alpha}_i Q_k(\mathbf{x}^\top \bar{\mathbf{x}}_i) \quad (35)$$

where again $\bar{\alpha}_i \sim \mathcal{B}(1/2)$ and $\bar{\mathbf{x}}_i \sim p(\mathbf{x})$ are sampled randomly. Figure 3(a) shows the learning curve for a fully connected two layer ReLU network with width $N = 10000$, input dimension $d = 30$ and $P' = 10000$. As before, we see that the lower k pure modes require less data to be fit. Experimental test errors for kernel regression with NTK on

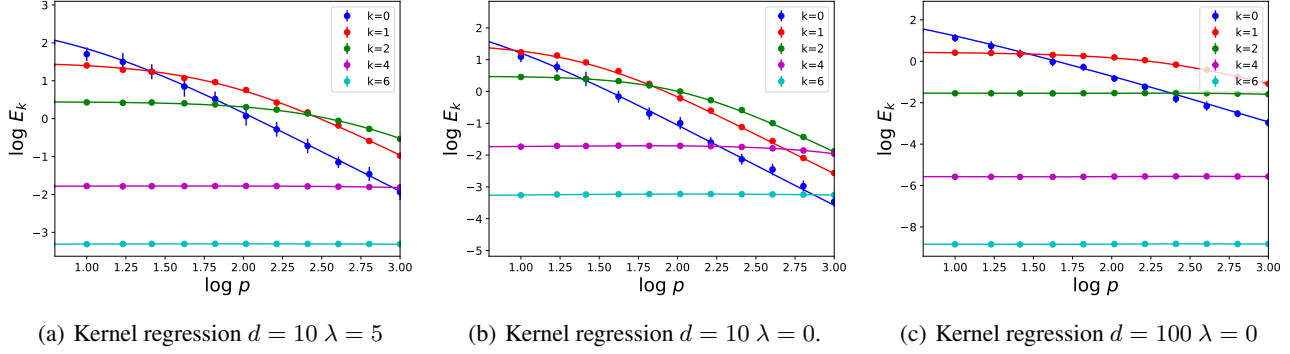


Figure 2. Mode errors for kernel regression and interpolation with NTK compared to theory. Solid lines are theoretical curves calculated using equation (21). Errorbars show standard deviation across the 50 trials. Logarithms are evaluated with base 10.

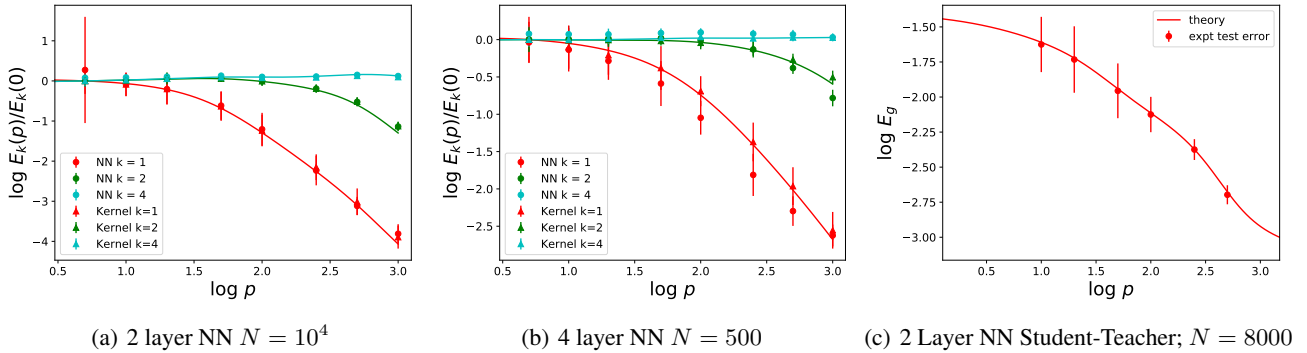


Figure 3. Learning curves for neural networks on “pure modes” as defined in eq. (35) as well as the learning curve for the student teacher setup defined in (36). The theory curves shown as solid lines are again computed with eq. (21). The test error for the finite width neural networks and NTK are shown with dots and triangles respectively. The generalization error was estimated by taking a random test sample of 1000 data points. The average was taken over 25 trials and the standard deviations are shown with errorbars. The networks were initialized with the default Gaussian NTK parameterization (Jacot et al., 2018) and trained with stochastic gradient descent (details in SI Section 12). Logarithms are evaluated with base 10.

the same synthetic datasets are plotted as triangles. Our theory perfectly fits the experiments.

Results from a 4-layer NN simulation are provided in Figure 3(b). Each hidden layer had $N = 500$ hidden units. We again see that the $k = 2$ mode is only learned for $p > 200$. $k = 4$ mode is not learned at all in this range. Our theory again perfectly fits the experiments.

Lastly we show that our theory also works for composite functions that contain many different degree spherical harmonics. In this setup, we randomly initialize a two layer teacher neural network and train a student neural network

$$f^*(\mathbf{x}) = \bar{\mathbf{r}}^\top \sigma(\bar{\Theta} \mathbf{x}), \quad f(\mathbf{x}) = \mathbf{r}^\top \sigma(\Theta \mathbf{x}), \quad (36)$$

where $\Theta, \bar{\Theta} \in \mathbb{R}^{M \times d}$ are the feedforward weights for the student and teacher respectively and $\mathbf{r}, \bar{\mathbf{r}} \in \mathbb{R}^M$ are the student and teacher readout weights. Chosen in this way with ReLU activations, the teacher is composed of spherical harmonics of many different degrees (Section 12 in SI). The total generalization error for this teacher student setup as

well as the theoretical prediction of our theory is provided in Figure 3(c) for $d = 25$, $N = 8000$. They agree excellently. Results from additional neural network simulations are provided in Section 12 of the SI.

5. Discussion and Conclusion

In this paper, we presented an approximate theory of the average generalization performance for kernel regression. We studied our theory in the ridgeless limit to explain the behavior of trained neural networks in the infinite width limit (Jacot et al., 2018; Arora et al., 2019). Our theory demonstrates how the RKHS eigenspectrum of NTK encodes a preferential bias to learn high frequency modes only after the sample size p is sufficiently large. Our theory fits kernel regression experiments remarkably well. We further experimentally verified that the theoretical learning curves obtained in the infinite width limit provide a good approximation of the learning curves for wide but finite NNs.

Acknowledgements

C. Pehlevan acknowledges support by the NIH and Intel Corporation.

References

- Abramowitz, M. and Stegun, I. A. *Handbook of Mathematical Functions with Formulas, Graphs, and Mathematical Tables*. Dover, New York, ninth dover printing, tenth gpo printing edition, 1964.
- Advani, M., Lahiri, S., and Ganguli, S. Statistical mechanics of complex neural systems and high dimensional data. *Journal of Statistical Mechanics: Theory and Experiment*, 2013(03):P03014, Mar 2013.
- Arfken, G. *Mathematical Methods for Physicists*. Academic Press, Inc., San Diego, third edition, 1985.
- Arora, S., Du, S. S., Hu, W., Li, Z., Salakhutdinov, R. R., and Wang, R. On exact computation with an infinitely wide neural net. In *Advances in Neural Information Processing Systems*, pp. 8139–8148, 2019.
- Belkin, M., Hsu, D., Ma, S., and Mandal, S. Reconciling modern machine learning practice and the bias-variance trade-off, 2018a.
- Belkin, M., Hsu, D. J., and Mitra, P. Overfitting or perfect fitting? risk bounds for classification and regression rules that interpolate. In Bengio, S., Wallach, H., Larochelle, H., Grauman, K., Cesa-Bianchi, N., and Garnett, R. (eds.), *Advances in Neural Information Processing Systems 31*, pp. 2300–2311. Curran Associates, Inc., 2018b.
- Belkin, M., Ma, S., and Mandal, S. To understand deep learning we need to understand kernel learning, 2018c.
- Belkin, M., Rakhlin, A., and Tsybakov, A. B. Does data interpolation contradict statistical optimality? In Chaudhuri, K. and Sugiyama, M. (eds.), *Proceedings of Machine Learning Research*, volume 89 of *Proceedings of Machine Learning Research*, pp. 1611–1619. PMLR, 16–18 Apr 2019.
- Bietti, A. and Mairal, J. On the inductive bias of neural tangent kernels, 2019.
- Cao, Y., Fang, Z., Wu, Y., Zhou, D.-X., and Gu, Q. Towards understanding the spectral bias of deep learning, 2019.
- Cohen, O., Malka, O., and Ringel, Z. Learning curves for deep neural networks: A gaussian field theory perspective, 2019.
- Cucker, F. and Smale, S. Best choices for regularization parameters in learning theory: On the bias-variance problem. *Foundations of Computational Mathematics*, 2:413–428, 01 2002.
- Dai, F. and Xu, Y. *Approximation Theory and Harmonic Analysis on Spheres and Balls*. Springer New York, 2013.
- Dietrich, R., Oppen, M., and Sompolinsky, H. Statistical mechanics of support vector networks. *Physical Review Letters*, 82(14):29752978, Apr 1999.
- Efthimiou, C. and Frye, C. *Spherical Harmonics In P Dimensions*. World Scientific Publishing Company, 2014.
- Engel, A. and Van den Broeck, C. *Statistical mechanics of learning*. Cambridge University Press, 2001.
- Evgeniou, T., Pontil, M., and Poggio, T. Regularization networks and support vector machines. *Advances in Computational Mathematics - Adv. Comput. Math.*, 13, 11 1999.
- Gyorfi, L., Kohler, M., Krzyzak, A., and Walk, H. A distribution-free theory of nonparametric regression. *Journal of the American Statistical Association*, 98(464): 1084–1084, 2003. doi: 10.1198/jasa.2003.s309.
- Hubbard, J. Calculation of partition functions. *Phys. Rev. Lett.*, 3:77–78, Jul 1959. doi: 10.1103/PhysRevLett.3.77.
- Jacot, A., Gabriel, F., and Hongler, C. Neural tangent kernel: Convergence and generalization in neural networks, 2018.
- LeCun, Y., Bengio, Y., and Hinton, G. Deep learning. *nature*, 521(7553):436–444, 2015.
- Lee, J., Xiao, L., Schoenholz, S., Bahri, Y., Novak, R., Sohl-Dickstein, J., and Pennington, J. Wide neural networks of any depth evolve as linear models under gradient descent. In *Advances in neural information processing systems*, pp. 8570–8581, 2019.
- Liang, T. and Rakhlin, A. Just interpolate: Kernel ”ridgeless” regression can generalize, 2018.
- Luo, T., Ma, Z., Xu, Z. J., and Zhang, Y. Theory of the frequency principle for general deep neural networks. *CoRR*, abs/1906.09235, 2019.
- Mercer, J. Xvi. functions of positive and negative type, and their connection the theory of integral equations. *Philosophical transactions of the royal society of London. Series A, containing papers of a mathematical or physical character*, 209(441-458):415–446, 1909.
- Mézard, M., Parisi, G., and Virasoro, M. *Spin glass theory and beyond: An Introduction to the Replica Method and Its Applications*, volume 9. World Scientific Publishing Company, 1987.
- Novak, R., Xiao, L., Hron, J., Lee, J., Alemi, A. A., Sohl-Dickstein, J., and Schoenholz, S. S. Neural tangents: Fast and easy infinite neural networks in python.

In *International Conference on Learning Representations*, 2020. URL <https://github.com/google/neural-tangents>.

Opper, M. and Vivarelli, F. General bounds on bayes errors for regression with gaussian processes. In Kearns, M. J., Solla, S. A., and Cohn, D. A. (eds.), *Advances in Neural Information Processing Systems 11*, pp. 302–308. MIT Press, 1999.

Rahaman, N., Baratin, A., Arpit, D., Draxler, F., Lin, M., Hamprecht, F. A., Bengio, Y., and Courville, A. On the spectral bias of neural networks, 2018.

Rasmussen, C. E. and Williams, C. K. I. *Gaussian Processes for Machine Learning (Adaptive Computation and Machine Learning)*. The MIT Press, 2005.

Scholkopf, B. and Smola, A. J. *Learning with Kernels: Support Vector Machines, Regularization, Optimization, and Beyond*. MIT Press, Cambridge, MA, USA, 2001. ISBN 0262194759.

Sherrington, D. and Kirkpatrick, S. Solvable model of a spin-glass. *Phys. Rev. Lett.*, 35:1792–1796, Dec 1975. doi: 10.1103/PhysRevLett.35.1792.

Smola, A. J., Óvári, Z. L., and Williamson, R. C. Regularization with dot-product kernels. In Leen, T. K., Dietterich, T. G., and Tresp, V. (eds.), *Advances in Neural Information Processing Systems 13*, pp. 308–314. MIT Press, 2001.

Sollich, P. Learning curves for gaussian processes. In *Advances in neural information processing systems*, pp. 344–350, 1999.

Sollich, P. Gaussian process regression with mismatched models. In *Advances in Neural Information Processing Systems*, pp. 519–526, 2002.

Sollich, P. and Halees, A. Learning curves for gaussian process regression: Approximations and bounds. *Neural Computation*, 14(6):1393–1428, Jun 2002.

Vapnik, V. N. An overview of statistical learning theory. *IEEE transactions on neural networks*, 10(5):988–999, 1999.

Wahba, G. *Spline Models for Observational Data*. Society for Industrial and Applied Mathematics, Philadelphia, 1990.

Yang, G. and Salman, H. A fine-grained spectral perspective on neural networks, 2019.

Supplementary Information (SI)

1. Background on Kernel Machines

1.1. Reproducing Kernel Hilbert Space

Let $\mathcal{X} \subseteq \mathbb{R}^d$ and $p(\mathbf{x})$ be a probability distribution over \mathcal{X} . Let \mathcal{H} be a Hilbert space with inner product $\langle \cdot, \cdot \rangle_{\mathcal{H}}$. A kernel $K(\cdot, \cdot)$ is said to be reproducing for \mathcal{H} if function evaluation at any $\mathbf{x} \in \mathcal{X}$ is the equivalent to the Hilbert inner product with $K(\cdot, \mathbf{x})$: K is reproducing for \mathcal{H} if for all $g \in \mathcal{H}$ and all $\mathbf{x} \in \mathcal{X}$

$$\langle K(\cdot, \mathbf{x}), g \rangle_{\mathcal{H}} = g(\mathbf{x}). \quad (\text{SI.1})$$

If such a kernel exists for a Hilbert space, then it is unique and defined as the reproducing kernel for the RKHS (Evgeniou et al., 1999; Scholkopf & Smola, 2001).

1.2. Mercer’s Theorem

Let \mathcal{H} be a RKHS with kernel K . Mercer’s theorem (Mercer, 1909; Rasmussen & Williams, 2005) allows the eigendecomposition of K

$$K(\mathbf{x}, \mathbf{x}') = \sum_{\rho} \lambda_{\rho} \phi_{\rho}(\mathbf{x}) \phi_{\rho}(\mathbf{x}'), \quad (\text{SI.2})$$

where the eigenvalue statement is

$$\int d\mathbf{x}' p(\mathbf{x}') K(\mathbf{x}, \mathbf{x}') \phi_{\rho}(\mathbf{x}') = \lambda_{\rho} \phi_{\rho}(\mathbf{x}). \quad (\text{SI.3})$$

1.3. Representer Theorem

Let \mathcal{H} be a RKHS with inner product $\langle \cdot, \cdot \rangle_{\mathcal{H}}$. Consider the regularized learning problem

$$\min_{f \in \mathcal{H}} \hat{\mathcal{L}}[f] + \lambda \|f\|_{\mathcal{H}}^2, \quad (\text{SI.4})$$

where $\hat{\mathcal{L}}[f]$ is an empirical cost defined on the discrete support of the dataset and $\lambda > 0$. The optimal solution to the optimization problem above can always be written as (Scholkopf & Smola, 2001)

$$f(x) = \sum_{i=1}^p \alpha_i K(x_i, x). \quad (\text{SI.5})$$

1.4. Solution to Least Squares

Specializing to the case of least squares regression, let

$$\hat{\mathcal{L}}[f] = \sum_{i=1}^p (f(\mathbf{x}_i) - y_i)^2. \quad (\text{SI.6})$$

Using the representer theorem, we may reformulate the entire objective in terms of the p coefficients α_i

$$\begin{aligned}\mathcal{L}[f] &= \sum_{i=1}^p (f(\mathbf{x}_i) - y_i)^2 + \lambda \|f\|_{\mathcal{H}}^2 \\ &= \sum_{i=1}^p \left(\sum_{j=1}^p \alpha_j K(\mathbf{x}_i, \mathbf{x}_j) - y_i \right)^2 \\ &\quad + \lambda \sum_{ij} \alpha_i \alpha_j \langle K(\mathbf{x}_i, \cdot), K(\mathbf{x}_j, \cdot) \rangle \\ &= \boldsymbol{\alpha}^\top \mathbf{K}^2 \boldsymbol{\alpha} - 2\mathbf{y}^\top \mathbf{K} \boldsymbol{\alpha} + \mathbf{y}^\top \mathbf{y} + \lambda \boldsymbol{\alpha}^\top \mathbf{K} \boldsymbol{\alpha}. \quad (\text{SI.7})\end{aligned}$$

Optimizing this loss with respect to $\boldsymbol{\alpha}$ gives

$$\boldsymbol{\alpha} = (\mathbf{K} + \lambda \mathbf{I})^{-1} \mathbf{y}. \quad (\text{SI.8})$$

Therefore the optimal function evaluated at a test point is

$$f(\mathbf{x}) = \boldsymbol{\alpha}^\top \mathbf{k}(\mathbf{x}) = \mathbf{y}^\top (\mathbf{K} + \lambda \mathbf{I})^{-1} \mathbf{k}(\mathbf{x}). \quad (\text{SI.9})$$

2. Derivation of the Generalization Error

Let the RKHS \mathcal{H} have eigenvalues λ_ρ for $\rho \in \mathbb{Z}^+$. Define $\psi_\rho(\mathbf{x}) = \sqrt{\lambda_\rho} \phi_\rho(\mathbf{x})$, where ϕ_ρ are the eigenfunctions of the reproducing kernel for \mathcal{H} . Let the target function have the following expansion in terms of the kernel eigenfunctions $f^*(\mathbf{x}) = \sum_\rho \bar{w}_\rho \psi_\rho(\mathbf{x})$. Define the design matrices $\Phi_{\rho,i} = \phi_\rho(\mathbf{x}_i)$ and $\Lambda_{\rho\gamma} = \lambda_\rho \delta_{\rho\gamma}$. Then the average generalization error for kernel regression is

$$E_g = \text{Tr} \left(\mathbf{D} \langle \mathbf{G}^2 \rangle_{\{\mathbf{x}_i\}} \right) \quad (\text{SI.10})$$

where

$$\mathbf{G} = \left(\frac{1}{\lambda} \Phi \Phi^\top + \Lambda^{-1} \right)^{-1}, \quad \Phi = \Lambda^{-1/2} \Psi. \quad (\text{SI.11})$$

and

$$\mathbf{D} = \Lambda^{-1/2} \langle \bar{\mathbf{w}} \bar{\mathbf{w}}^\top \rangle_{\bar{\mathbf{w}}} \Lambda^{-1/2}. \quad (\text{SI.12})$$

Proof. Define the student's eigenfunction expansion $f(\mathbf{x}) = \sum_\rho w_\rho \psi_\rho(\mathbf{x})$ and decompose the risk in the basis of eigenfunctions:

$$\begin{aligned}E_g(\{\mathbf{x}_i\}, f^*) &= \langle (f(\mathbf{x}) - y(\mathbf{x}))^2 \rangle_x \\ &= \sum_{\rho, \gamma} (w_\rho - \bar{w}_\rho)(w_\gamma - \bar{w}_\gamma) \langle \psi_\rho(\mathbf{x}) \psi_\gamma(\mathbf{x}) \rangle \\ &= \sum_\rho \lambda_\rho (w_\rho - \bar{w}_\rho)^2 \\ &= (\mathbf{w} - \bar{\mathbf{w}})^\top \Lambda (\mathbf{w} - \bar{\mathbf{w}}). \quad (\text{SI.13})\end{aligned}$$

Next, it suffices to calculate the weights \mathbf{w} learned through kernel regression. Define a matrix with elements $\Psi_{\rho,i} = \psi_\rho(\mathbf{x}_i)$. The training error for kernel regression is

$$E_{tr} = \|\Psi^\top \mathbf{w} - \mathbf{y}\|^2 + \lambda \|\mathbf{w}\|_2^2 \quad (\text{SI.14})$$

The ℓ_2 norm on \mathbf{w} is equivalent to the Hilbert norm on the student function. If $f(\mathbf{x}) = \sum_\rho w_\rho \psi_\rho(\mathbf{x})$ then

$$\begin{aligned}\|f\|_{\mathcal{H}}^2 &= \langle f, f \rangle_{\mathcal{H}} \\ &= \sum_{\rho, \gamma} w_\rho w_\gamma \langle \psi_\rho, \psi_\gamma \rangle_{\mathcal{H}} = \sum_\rho w_\rho^2, \quad (\text{SI.15})\end{aligned}$$

since $\langle \psi_\rho, \psi_\gamma \rangle_{\mathcal{H}} = \delta_{\rho, \gamma}$ (Bietti & Mairal, 2019). The training error has a unique minimum

$$\begin{aligned}\mathbf{w} &= (\Psi \Psi^\top + \lambda \mathbf{I})^{-1} \Psi \mathbf{y} = (\Psi \Psi^\top + \lambda \mathbf{I})^{-1} \Psi \Psi^\top \bar{\mathbf{w}} \\ &= \bar{\mathbf{w}} - \lambda (\Psi \Psi^\top + \lambda \mathbf{I})^{-1} \bar{\mathbf{w}}, \quad (\text{SI.16})\end{aligned}$$

where the target function is produced according to $\mathbf{y} = \Psi^\top \bar{\mathbf{w}}$.

Plugging in the \mathbf{w} that minimizes the training error into the formula for the generalization error, we find

$$E_g(\{\mathbf{x}_i\}, \bar{\mathbf{w}}) = \lambda^2 \langle \bar{\mathbf{w}} (\Psi \Psi^\top + \lambda \mathbf{I})^{-1} \Lambda (\Psi \Psi^\top + \lambda \mathbf{I})^{-1} \bar{\mathbf{w}} \rangle. \quad (\text{SI.17})$$

Defining

$$\mathbf{G} = \lambda \Lambda^{1/2} (\Psi \Psi^\top + \lambda \mathbf{I})^{-1} \Lambda^{1/2} = \left(\frac{1}{\lambda} \Phi \Phi^\top + \Lambda^{-1} \right)^{-1}, \quad (\text{SI.18})$$

and

$$\mathbf{D} = \Lambda^{-1/2} \langle \bar{\mathbf{w}} \bar{\mathbf{w}}^\top \rangle_{\bar{\mathbf{w}}} \Lambda^{-1/2}, \quad (\text{SI.19})$$

and identifying the terms in (SI.17) with these definitions, we obtain the desired result. Then each component of the mode error is given by:

$$E_\rho = \sum_\gamma \mathbf{D}_{\rho, \gamma} \langle \mathbf{G}_{\gamma, \rho}^2 \rangle \quad (\text{SI.20})$$

□

3. Solution of the PDE Using Method of Characteristics

Here we derive the solution to the PDE in equation (17) of the main text by adapting the method used by (Sollich, 1999). We will prove both Propositions 2 and 3.

Let

$$g_\rho(p, v) \equiv \langle \tilde{\mathbf{G}}(p, v)_{\rho\rho} \rangle, \quad (\text{SI.21})$$

and

$$t(p, v) \equiv \text{Tr} \langle \mathbf{G}(p, v) \rangle = \sum_\rho g_\rho(p, v). \quad (\text{SI.22})$$

It follows from equation (17) that t obeys the PDE

$$\frac{\partial t(p, v)}{\partial p} = \frac{1}{\lambda + t} \frac{\partial t(p, v)}{\partial v}, \quad (\text{SI.23})$$

with an initial condition $t(0, v) = \text{Tr}(\mathbf{\Lambda}^{-1} + v\mathbf{I})^{-1}$. The solution to first order PDEs of the form is given by the method of characteristics (Arfken, 1985), which we describe below, and prove Proposition 2.

Proof of Proposition 2. The solution to (SI.23) is a surface $(t, p, v) \subset \mathbb{R}^3$ that passes through the line $(\text{Tr}(\mathbf{\Lambda}^{-1} + v\mathbf{I})^{-1}, 0, v)$ and satisfies the PDE at all points. The tangent plane to the solution surface at a point (t, p, v) is $\text{span}\{(\frac{\partial t}{\partial p}, 1, 0), (\frac{\partial t}{\partial v}, 0, 1)\}$. Therefore a vector $\mathbf{a} = (a_t, a_p, a_v) \in \mathbb{R}^3$ normal to the solution surface must satisfy

$$a_t \frac{\partial t}{\partial p} + a_p = 0, \quad a_t \frac{\partial t}{\partial v} + a_v = 0.$$

One such normal vector is $(-1, \frac{\partial t}{\partial p}, \frac{\partial t}{\partial v})$.

The PDE can be written as a dot product involving this normal vector,

$$\left(-1, \frac{\partial t}{\partial p}, \frac{\partial t}{\partial v}\right) \cdot \left(0, 1, -\frac{1}{\lambda + t}\right) = 0, \quad (\text{SI.24})$$

demonstrating that $(0, 1, -\frac{1}{\lambda + t})$ is tangent to the solution surface. This allows us to parameterize one dimensional curves along the solution in these tangent directions. Such curves are known as characteristics. Introducing a parameter $s \in \mathbb{R}$ that varies along the one dimensional characteristic curves, we get

$$\frac{dt}{ds} = 0, \quad \frac{dp}{ds} = 1, \quad \frac{dv}{ds} = -\frac{1}{\lambda + t}. \quad (\text{SI.25})$$

The first of these equations indicate that t is constant along each characteristic curve. Integrating along the parameter, $p = s + p_0$ and $v = -\frac{s}{\lambda + t} + v_0$ where p_0 is the value of p when $s = 0$ and v_0 is the value of v at $s = 0$. Without loss of generality, take $p_0 = 0$ so that $s = p$. At $s = 0$, we have our initial condition

$$t(0, v) = \text{Tr}(\mathbf{\Lambda}^{-1} + v_0\mathbf{I})^{-1}. \quad (\text{SI.26})$$

Since t takes on the same value for each characteristic

$$t(p, v) = \text{Tr}\left(\mathbf{\Lambda}^{-1} + \left(v + \frac{p}{\lambda + t(p, v)}\right)\mathbf{I}\right)^{-1}, \quad (\text{SI.27})$$

which gives an implicit solution for $t(p, v)$. Now that we have solved for $t(p, v)$, remembering (SI.22), we may write

$$g_\rho(p, v) = \left(\frac{1}{\lambda_\rho} + v + \frac{p}{\lambda + t(p, v)}\right)^{-1}. \quad (\text{SI.28})$$

This equation proves Proposition 2 of the main text. \square

Next, we compute the modal generalization errors E_ρ and prove Proposition 3.

Proof of Proposition 3. Computing generalization error of kernel regression requires the differentiation with respect to v at $v = 0$ (equations (11) and (16) of main text). Since $\langle \mathbf{G}^2 \rangle$ is diagonal, the mode errors only depend on the diagonals of \mathbf{D} and on $\langle \mathbf{G}_{\rho, \rho}^2 \rangle = -\frac{\partial g_\rho}{\partial v}|_{v=0}$:

$$E_\rho = \sum_\gamma \mathbf{D}_{\rho, \gamma} \langle \mathbf{G}_{\gamma, \rho}^2 \rangle = -\frac{\langle \bar{w}_\rho^2 \rangle}{\lambda_\rho} \frac{\partial g_\rho}{\partial v} \Big|_{v=0}. \quad (\text{SI.29})$$

We proceed with calculating the derivative in the above equation.

$$\begin{aligned} \frac{\partial g_\rho(p, 0)}{\partial v} &= -\left(\frac{1}{\lambda_\rho} + \frac{p}{\lambda + t(p, 0)}\right)^{-2} \\ &\quad \times \left(1 - \frac{p}{(\lambda + t)^2} \frac{\partial t(p, 0)}{\partial v}\right). \end{aligned} \quad (\text{SI.30})$$

We need to calculate $\frac{\partial t(p, v)}{\partial v}|_{v=0}$

$$\frac{\partial t(p, 0)}{\partial v} = -\gamma \left(1 - \frac{p}{(\lambda + t)^2} \frac{\partial t(p, 0)}{\partial v}\right), \quad (\text{SI.31})$$

where

$$\gamma \equiv \sum_\rho \left(\frac{1}{\lambda_\rho} + \frac{p}{\lambda + t(p, 0)}\right)^{-2}. \quad (\text{SI.32})$$

Solving for the derivative, we get

$$\frac{\partial t(p, 0)}{\partial v} = -\frac{\gamma}{1 - \gamma \frac{p}{(\lambda + t)^2}}, \quad (\text{SI.33})$$

and

$$\frac{\partial g_\rho(p, 0)}{\partial v} = -\left(\frac{1}{\lambda_\rho} + \frac{p}{\lambda + t}\right)^{-2} \left(1 - \frac{\gamma p}{(\lambda + t)^2}\right)^{-1}. \quad (\text{SI.34})$$

The error in mode ρ is therefore

$$E_\rho = \frac{\langle \bar{w}_\rho^2 \rangle}{\lambda_\rho} \left(\frac{1}{\lambda_\rho} + \frac{p}{\lambda + t(p)}\right)^{-2} \left(1 - \frac{p\gamma(p)}{(\lambda + t(p))^2}\right)^{-1}, \quad (\text{SI.35})$$

so it suffices to numerically solve for $t(p, 0)$ to recover predictions of the mode errors. Equations (SI.27) (evaluated at $v = 0$), (SI.32) and (SI.35) collectively prove Proposition 3. \square

4. Replica Calculation

In this section, we present the replica trick and the saddle-point approximation summarized in main text Section 2.3. Our goal is to show that the continuous approximation of the main paper and previous section can be interpreted as

a finite size saddle-point approximation to the replicated system under a replica decoupled ansatz. We will present a detailed treatment of the thermodynamic limit and the replica symmetric ansatz in a different paper.

Let $\tilde{\mathbf{G}}(p, v, \chi) = (\frac{1}{\chi} \mathbf{\Phi} \mathbf{\Phi}^\top + \mathbf{\Lambda}^{-1} + v \mathbf{I} + \chi \mathbf{D})^{-1}$. Then, the generalization error is

$$\begin{aligned} E_g &= \left\langle \text{Tr} \left(\mathbf{D} \tilde{\mathbf{G}}(p, v, \chi)^2 \right) \right\rangle \\ &= -\frac{\partial}{\partial \chi} \left\langle \text{Tr} \tilde{\mathbf{G}}(p, v, \chi) \right\rangle \\ &= -\frac{\partial^2}{\partial v \partial \chi} \left\langle \text{Tr} \log \left(\tilde{\mathbf{G}}(p, v, \chi)^{-1} \right) \right\rangle \\ &= 2 \frac{\partial^2}{\partial v \partial \chi} \left\langle \log \left(\det \tilde{\mathbf{G}}(p, v, \chi)^{1/2} \right) \right\rangle. \end{aligned} \quad (\text{SI.36})$$

In this form, we can recognize the partition function

$$Z = \det \left(\frac{1}{\chi} \mathbf{\Phi} \mathbf{\Phi}^\top + \mathbf{\Lambda}^{-1} + v \mathbf{I} + \chi \mathbf{D} \right)^{-1/2}. \quad (\text{SI.37})$$

To calculate the average $\langle \log Z \rangle$, we will use the replica trick (Mézard et al., 1987):

$$\langle \log Z \rangle = \lim_{n \rightarrow 0} \frac{\langle Z^n \rangle - 1}{n}. \quad (\text{SI.38})$$

We will calculate $\langle Z^n \rangle$ for integer powers and take the limit $n \rightarrow 0$ by analytical continuation. This is a non-rigorous, but a standard technique in the physics of disordered systems (Mézard et al., 1987; Engel & Van den Broeck, 2001).

Following (Advani et al., 2013), we represent the determinant as a Gaussian integral

$$Z = \int \frac{d\mathbf{u}}{\sqrt{(2\pi)^M}} e^{-\frac{1}{2} \mathbf{u}^\top (\frac{1}{\chi} \mathbf{\Phi} \mathbf{\Phi}^\top + \mathbf{\Lambda}^{-1} + v \mathbf{I} + \chi \mathbf{D}) \mathbf{u}}, \quad (\text{SI.39})$$

and replicate

$$\begin{aligned} \langle Z^n \rangle &= \int \prod_a \frac{d\mathbf{u}^a}{\sqrt{(2\pi)^M}} \left\langle e^{-\frac{1}{2} \sum_a \mathbf{u}^{a\top} (\frac{1}{\chi} \mathbf{\Phi} \mathbf{\Phi}^\top + \mathbf{\Lambda}^{-1} + v \mathbf{I} + \chi \mathbf{D}) \mathbf{u}^a} \right\rangle. \end{aligned} \quad (\text{SI.40})$$

To perform the average, we will resort to a Gaussian approximation. For this purpose we introduce variables

$$\gamma_i^a = \sum_\rho u_\rho^a \phi_\rho(\mathbf{x}_i), \quad (\text{SI.41})$$

which have covariance structure

$$\begin{aligned} \langle \gamma_i^a \gamma_j^b \rangle &= \sum_\rho \sum_\gamma \langle \phi_\rho(x_i) \phi_\gamma(x_j) \rangle u_\rho^a u_\gamma^b \\ &= \delta_{ij} \mathbf{u}^a \cdot \mathbf{u}^b = \delta_{ij} Q_{ab}. \end{aligned} \quad (\text{SI.42})$$

The order parameters $Q_{ab} = \mathbf{u}^a \cdot \mathbf{u}^b$ represent overlap of the degrees of freedom between replicas a and b . To simplify the remainder of the calculation, we will study the case where all features are zero mean $\langle \phi_\rho(\mathbf{x}) \rangle_{\mathbf{x}}$ which implies that the variables γ_i^a are also zero mean. Including a zero-frequency constant offset in the RKHS produces a slight modification in the final error for the zero-frequency mode. This addition complicates the expressions while adding little conceptual insight.

Since γ_i^a is a sum of many terms, we will approximate the distribution over γ_i^a as jointly Gaussian. The average over the sampled data $\{\mathbf{x}_i\}$ will be replaced with an average over the γ_i variables. Further, since they decouple over different data points, it suffices to compute a single average

$$\left\langle e^{-\frac{1}{2\chi} \sum_a \mathbf{u}^a \mathbf{\Phi} \mathbf{\Phi}^\top \mathbf{u}^a} \right\rangle = \left[\left\langle e^{-\frac{1}{2\chi} \sum_a \gamma_a^2} \right\rangle_\gamma \right]^p, \quad (\text{SI.43})$$

and

$$\begin{aligned} \left\langle e^{-\frac{1}{2\chi} \sum_a \gamma_a^2} \right\rangle_\gamma &= \int \frac{d\gamma}{\sqrt{(2\pi)^n \det \mathbf{Q}}} e^{-\frac{1}{2} \gamma^\top (\mathbf{Q}^{-1} + \frac{1}{\chi} \mathbf{I}) \gamma} \\ &= e^{-\frac{1}{2} \log \det (\mathbf{I} + \frac{1}{\chi} \mathbf{Q})}. \end{aligned} \quad (\text{SI.44})$$

After averaging over the training points, the replicated partition function can be rewritten

$$\begin{aligned} \langle Z^n \rangle &= \int \prod_a \frac{d\mathbf{u}^a}{\sqrt{(2\pi)^M}} \prod_{ab} dQ_{ab} \prod_{ab} d\hat{Q}_{ab} \\ &\quad \times e^{i \sum_{ab} \hat{Q}_{ab} \mathbf{u}^a \cdot \mathbf{u}^b - i \sum_{ab} \hat{Q}_{ab} Q_{ab}} \\ &\quad \times e^{-\frac{p}{2} \log \det (\mathbf{I} + \frac{1}{\chi} \mathbf{Q}) - \frac{v}{2} \text{Tr}(\mathbf{Q})} \\ &\quad \times e^{-\sum_a \mathbf{u}^a (\mathbf{\Lambda}^{-1} + \chi \mathbf{D}) \mathbf{u}^a}. \end{aligned} \quad (\text{SI.45})$$

Now we need to perform the integrals over thermal degrees of freedom in each replica. This requires computing integrals of the form

$$\int \prod_a \frac{d\mathbf{u}^a}{\sqrt{(2\pi)^M}} e^{i \sum_{ab} \hat{Q}_{ab} \mathbf{u}^a \cdot \mathbf{u}^b - \frac{1}{2} \sum_a \mathbf{u}^a (\mathbf{\Lambda}^{-1} + \chi \mathbf{D}) \mathbf{u}^a}. \quad (\text{SI.46})$$

If \mathbf{D} is diagonal, then these integrals factorize over different modes ρ . To study the general case where \mathbf{D} is not diagonal, we use the Hubbard-Stratonovich transform (Hubbard, 1959) to linearize the terms involving \mathbf{D} :

$$e^{-\frac{\chi}{2} \mathbf{u}_a^\top \mathbf{D} \mathbf{u}_a} = \int \frac{d\mathbf{t}_a}{\sqrt{(2\pi)^M \det(\chi \mathbf{D})}} e^{-\frac{1}{2} \mathbf{t}_a^\top (\frac{1}{\chi} \mathbf{D}^{-1}) \mathbf{t}_a + i \mathbf{t}_a \cdot \mathbf{u}_a}. \quad (\text{SI.47})$$

Let $\mathbf{u}_\rho \in \mathbb{R}^n$ be a vector with elements $\mathbf{u}_{\rho,a} = u_{\rho,a}^a$. The integrals over thermal degrees of freedom now decouple

over different modes ρ :

$$\int d\mathbf{u}_\rho e^{-\frac{1}{2}\mathbf{u}_\rho(\frac{1}{\lambda_\rho}\mathbf{I}-2i\hat{\mathbf{Q}})\mathbf{u}_\rho+i\mathbf{t}_\rho\cdot\mathbf{u}_\rho} = e^{-\frac{1}{2}\log\det(\frac{1}{\lambda_\rho}\mathbf{I}-2i\hat{\mathbf{Q}})-\frac{1}{2}\mathbf{t}_\rho(\frac{1}{\lambda_\rho}\mathbf{I}-2i\hat{\mathbf{Q}})^{-1}\mathbf{t}_\rho}. \quad (\text{SI.48})$$

Let $\mathbf{t}^a \in \mathbb{R}^M$ and $\mathbf{t}_\rho \in \mathbb{R}^n$ be rows and columns of the matrix that has elements t_ρ^a . The replicated partition function can now be written as:

$$\begin{aligned} \langle Z^n \rangle &= \int \prod_{ab} dQ_{ab} \prod_{ab} d\hat{Q}_{ab} e^{-i\sum_{ab} \hat{Q}_{ab} Q_{ab}} \\ &\times e^{-\frac{n}{2}\log\det(\mathbf{I}+\frac{1}{\lambda}\mathbf{Q})-\frac{n}{2}\text{Tr}(\mathbf{Q})} \\ &\times e^{-\frac{1}{2}\sum_\rho \log\det(\frac{1}{\lambda_\rho}\mathbf{I}-2i\hat{\mathbf{Q}})} e^{-\frac{n}{2}\log\det(\chi\mathbf{D})} \\ &\times \int \prod_{a\rho} \frac{dt_\rho^a}{\sqrt{2\pi}} e^{-\frac{1}{2}\sum_a \mathbf{t}^a(\frac{1}{\chi}\mathbf{D}^{-1})\mathbf{t}^a - \frac{1}{2}\sum_\rho \mathbf{t}_\rho(\frac{1}{\lambda_\rho}\mathbf{I}-2i\hat{\mathbf{Q}})^{-1}\mathbf{t}_\rho}. \end{aligned} \quad (\text{SI.49})$$

We will approximate this integral with a saddle point approximation. To evaluate the saddle point, we make a decoupled replica symmetric (RS) ansatz $Q_{ab} = q\delta_{ab}$ and $\hat{Q}_{ab} = \hat{q}\delta_{ab}$. While this is a strong assumption, even stronger than the replica symmetric ansatz (Mézard et al., 1987), it leads to the same results for generalization error as the continuous approximation. Therefore, we pursue it to demonstrate the correspondence between these two methods.

When we make this RS assumption, the terms involving matrices \mathbf{Q} and $\hat{\mathbf{Q}}$ simplify

$$\begin{aligned} \log\det\left(\mathbf{I}+\frac{1}{\lambda}\mathbf{Q}\right) &= n\log\left(1+\frac{q}{\lambda}\right), \\ \text{Tr}\mathbf{Q} &= nq, \\ \log\det\left(\frac{1}{\lambda_\rho}\mathbf{I}-2i\hat{\mathbf{Q}}\right) &= n\log\left(\frac{1}{\lambda_\rho}-2i\hat{q}\right), \\ \left(\frac{1}{\lambda_\rho}\mathbf{I}-2i\hat{\mathbf{Q}}\right)^{-1} &= \left(\frac{1}{\lambda_\rho}-2i\hat{q}\right)^{-1}\mathbf{I}. \end{aligned} \quad (\text{SI.50})$$

Under this ansatz, the t integrals can be evaluated exactly. Then

$$\begin{aligned} \langle Z^n \rangle &= \int dq d\hat{q} e^{-inq\hat{q}-\frac{n}{2}\log(1+\frac{q}{\lambda})-\frac{vn}{2}q} \\ &\times e^{-\frac{n}{2}\sum_\rho \log(\frac{1}{\lambda_\rho}-2i\hat{q}+\chi\langle\bar{w}_\rho^2\rangle/\lambda_\rho)}. \end{aligned} \quad (\text{SI.51})$$

Under the RS assumption, the free energy $F(q, \hat{q})$ can be written as

$$\begin{aligned} F(q, \hat{q}) &= \log\left(1+\frac{q}{\lambda}\right) \\ &+ \frac{1}{p}\left(vq + \sum_\rho \log\left(\frac{1}{\lambda_\rho} + \chi\frac{\langle\bar{w}_\rho^2\rangle}{\lambda_\rho} - 2i\hat{q}\right) + 2iq\hat{q}\right). \end{aligned} \quad (\text{SI.52})$$

The saddle point equations are

$$\begin{aligned} \frac{p}{\lambda+q} + v + 2i\hat{q} &= 0, \\ -\sum_\rho \left(\frac{1}{\lambda_\rho} + \chi\frac{\langle\bar{w}_\rho^2\rangle}{\lambda_\rho} - 2i\hat{q}\right)^{-1} + q &= 0. \end{aligned} \quad (\text{SI.53})$$

Here, \hat{q} can be eliminated for q , yielding the following nonlinear equation for q

$$q = \left(\frac{1}{\lambda_\rho} + \chi\frac{\langle\bar{w}_\rho^2\rangle}{\lambda_\rho} + \frac{p}{\lambda+q} + v\right)^{-1}. \quad (\text{SI.54})$$

Note that the order parameter q , which represents the overlap between the degrees of freedom at the saddle point, is exactly the trace of $\langle\tilde{G}(p, v)\rangle$ when $\chi \rightarrow 0$, or variable t as defined in (SI.22).

The generalization error is

$$\begin{aligned} E_g &= 2\frac{\partial^2}{\partial\chi\partial v} \lim_{n\rightarrow 0} \frac{\partial}{\partial n} \langle Z^n \rangle \\ &= -\frac{\partial^2}{\partial\chi\partial v} F(q, v) \\ &= -\frac{\partial}{\partial\chi} q. \end{aligned} \quad (\text{SI.55})$$

The last derivative can be solved implicitly from (SI.54), which leads to

$$E_g = \sum_\rho \frac{\langle\bar{w}_\rho^2\rangle}{\lambda_\rho} \frac{(\lambda+q)^2}{(\frac{1}{\lambda_\rho} + \frac{p}{\lambda+q})^2[(\lambda+q)^2 - p\gamma]}, \quad (\text{SI.56})$$

where γ is defined as before in (SI.32) with the identification $t \rightarrow q$. This is exactly the generalization error obtained from the continuous approximation, equation (21).

5. Spherical Harmonics

Let $-\Delta$ represent the Laplace-Beltrami operator in \mathbb{R}^d . Spherical harmonics $\{Y_{km}\}$ in dimension d are harmonic ($-\Delta Y_{km}(\mathbf{x}) = 0$), homogenous ($Y_{km}(t\mathbf{x}) = t^k Y_{km}(\mathbf{x})$) polynomials that are orthonormal with respect to the uniform measure on \mathbb{S}^{d-1} (Efthimiou & Frye, 2014; Dai & Xu, 2013). The number of spherical harmonics of degree k in dimension d denoted by $N(d, k)$ is

$$N(d, k) = \frac{2k+d-2}{k} \binom{k+d-3}{k-1}. \quad (\text{SI.57})$$

The Laplace Beltrami Operator can be decomposed into the radial and angular parts, allowing

$$-\Delta = -\Delta_r - \Delta_{\mathbb{S}^{d-1}} \quad (\text{SI.58})$$

Using this decomposition, the spherical harmonics are eigenfunctions of the surface Laplacian

$$-\Delta_{\mathbb{S}^{d-1}} Y_{km}(\mathbf{x}) = k(k+d-2)Y_{km}(\mathbf{x}). \quad (\text{SI.59})$$

The spherical harmonics are related to the Gegenbauer polynomials $\{Q_k\}$, which are orthogonal with respect to the measure $d\tau(z) = (1-z^2)^{(d-3)/2}dz$ of inner products $z = \mathbf{x}^\top \mathbf{x}'$ of uniformly sampled pairs on the sphere $\mathbf{x}, \mathbf{x}' \sim \mathbb{S}^{d-1}$. The Gegenbauer polynomials can be constructed with the Gram-Schmidt procedure and have the following properties

$$Q_k(\mathbf{x}^\top \mathbf{x}') = \frac{1}{N(d, k)} \sum_{m=1}^{N(d, k)} Y_{km}(\mathbf{x}) Y_{km}(\mathbf{x}'),$$

$$\int_{-1}^1 Q_k(z) Q_\ell(z) d\tau(z) = \frac{\omega_{d-1}}{\omega_{d-2}} \frac{\delta_{k, \ell}}{N(d, k)}, \quad (\text{SI.60})$$

where $\omega_{d-1} = \frac{\pi^{d/2}}{\Gamma(d/2)}$ is the surface area of \mathbb{S}^{d-1} .

6. Decomposition of Dot Product Kernels on \mathbb{S}^{d-1}

For inputs sampled from the uniform measure on \mathbb{S}^{d-1} , dot product kernels can be decomposed into Gegenbauer polynomials introduced in SI Section 5.

Let $K(\mathbf{x}, \mathbf{x}') = \kappa(\mathbf{x}^\top \mathbf{x}')$. The kernel's orthogonal decomposition is

$$\kappa(z) = \sum_{k=0}^{\infty} \lambda_k N(d, k) Q_k(z),$$

$$\lambda_k = \frac{\omega_{d-2}}{\omega_{d-1}} \int_{-1}^1 \kappa(z) Q_k(z) d\tau(z). \quad (\text{SI.61})$$

To numerically calculate the kernel eigenvalues of κ , we use Gauss-Gegenbauer quadrature (Abramowitz & Stegun, 1964) for the measure $d\tau(z)$ so that for a quadrature scheme of order r

$$\int_{-1}^1 \kappa(z) Q_k(z) d\tau(z) \approx \sum_{i=1}^r w_i Q_k(z_i) \kappa(z_i), \quad (\text{SI.62})$$

where z_i are the r roots of $Q_r(z)$ and the weights w_i are chosen with

$$w_i = \frac{\Gamma(r + \alpha + 1)^2}{\Gamma(r + 2\alpha + 1)} \frac{2^{2r+2\alpha+1} r!}{V_r'(z_i) V_{r+1}(z_i)}, \quad (\text{SI.63})$$

where

$$V_r(z) = 2^r r! (-1)^r Q_r(z) \quad (\text{SI.64})$$

For our calculations we take $r = 1000$.

7. Neural Tangent Kernel

The neural tangent kernel is

$$K_{\text{NTK}}(\mathbf{x}, \mathbf{x}') = \sum_i \left\langle \frac{\partial f_\theta(\mathbf{x})}{\partial \theta_i} \frac{\partial f_\theta(\mathbf{x}')}{\partial \theta_i} \right\rangle_\theta. \quad (\text{SI.65})$$

For a neural network, it is convenient to compute this recursively in terms of the Neural Network Gaussian Process (NNGP) kernel which corresponds to only training the read-out weights from the final layer (Jacot et al., 2018; Arora et al., 2019). We will restrict our attention to networks with zero bias and nonlinear activation function σ . Then

$$K_{\text{NTK}}^{(1)}(\mathbf{x}, \mathbf{x}') = K_{\text{NNGP}}^{(1)}(\mathbf{x}, \mathbf{x}')$$

$$K_{\text{NTK}}^{(2)}(\mathbf{x}, \mathbf{x}') = K_{\text{NNGP}}^{(2)}(\mathbf{x}, \mathbf{x}') + K_{\text{NTK}}^{(1)}(\mathbf{x}, \mathbf{x}') \dot{K}^{(2)}(\mathbf{x}, \mathbf{x}')$$

$$\vdots$$

$$K_{\text{NTK}}^{(L)}(\mathbf{x}, \mathbf{x}') = K_{\text{NNGP}}^{(L)}(\mathbf{x}, \mathbf{x}') + K_{\text{NTK}}^{(L-1)}(\mathbf{x}, \mathbf{x}') \dot{K}^{(L)}(\mathbf{x}, \mathbf{x}'), \quad (\text{SI.66})$$

where

$$K_{\text{NNGP}}^{(L)}(\mathbf{x}, \mathbf{x}') = \mathbb{E}_{(\alpha, \beta) \sim p_{\mathbf{x}, \mathbf{x}'}^{(L-1)}} \sigma(\alpha) \sigma(\beta),$$

$$\dot{K}^{(L)}(\mathbf{x}, \mathbf{x}') = \mathbb{E}_{(\alpha, \beta) \sim p_{\mathbf{x}, \mathbf{x}'}^{(L-1)}} \dot{\sigma}(\alpha) \dot{\sigma}(\beta),$$

$$p_{\mathbf{x}, \mathbf{x}'}^{(L-1)} = \mathcal{N} \left(\begin{pmatrix} 0 \\ 0 \end{pmatrix}, \begin{pmatrix} K^{(L-1)}(\mathbf{x}, \mathbf{x}) & K^{(L-1)}(\mathbf{x}, \mathbf{x}') \\ K^{(L-1)}(\mathbf{x}, \mathbf{x}') & K^{(L-1)}(\mathbf{x}', \mathbf{x}') \end{pmatrix} \right),$$

$$K_{\text{NNGP}}^{(1)}(\mathbf{x}, \mathbf{x}') = \mathbf{x}^\top \mathbf{x}'. \quad (\text{SI.67})$$

If σ is chosen to be the ReLU activation, then we can analytically simplify the expression. Defining the following function

$$f(z) = \arccos \left(\frac{1}{\pi} \sqrt{1-z^2} + \left(1 - \frac{1}{\pi} \arccos(z) \right) z \right), \quad (\text{SI.68})$$

we obtain

$$K_{\text{NNGP}}^{(L)}(\mathbf{x}, \mathbf{x}') = \cos \left(f^{\circ(L-1)}(\mathbf{x}^\top \mathbf{x}') \right)$$

$$\dot{K}^{(L)}(\mathbf{x}, \mathbf{x}') = \left(1 - \frac{1}{\pi} f^{\circ(L-2)}(\mathbf{x}^\top \mathbf{x}') \right), \quad (\text{SI.69})$$

where $f^{\circ(L-1)}(z)$ is the function f composed into itself $L-1$ times.

This simplification gives an exact recursive formula to compute the kernel as a function of $z = \mathbf{x}^\top \mathbf{x}'$, which is what we use to compute the eigenspectrum with the quadrature scheme described in the previous section.

8. Spectra of Fully Connected ReLU NTK

A plot showing the RKHS spectra of fully connected ReLU NTK's of varying depth is shown in Figure SI.1. As the depth increases, the spectrum becomes more white, eventually, the kernel's trace $\langle K(\mathbf{x}, \mathbf{x}) \rangle_{\mathbf{x}} = \sum_k \lambda_k N(d, k)$ begins to diverge. Inference with such a kernel is equivalent to learning a function with infinite variance. Constraints on the variance of derivatives $\langle \|\nabla_{\mathbb{S}^{d-1}}^n f(\mathbf{x})\|^2 \rangle$ correspond to more restrictive constraints on the eigenspectrum of the RKHS. Specifically, $\lambda_k N(d, k) \sim \mathcal{O}(k^{-n-1/2})$ implies that the n -th gradient has finite variance $\langle \|\nabla_{\mathbb{S}^{d-1}}^n f(\mathbf{x})\|^2 \rangle < \infty$.

Proof. By the representer theorem, let $f(\mathbf{x}) = \sum_{i=1}^p \alpha_i K(\mathbf{x}, \mathbf{x}_i)$. By Green's theorem, the variance of the n -th derivative can be rewritten as

$$\begin{aligned} \langle \|\nabla_{\mathbb{S}^{d-1}}^n f(\mathbf{x})\|^2 \rangle &= \langle f(\mathbf{x}) (-\Delta_{\mathbb{S}^{d-1}})^n f(\mathbf{x}) \rangle \\ &= \sum_{kk'mm'ij} \alpha_i \alpha_j \lambda_k \lambda_{k'} Y_{km}(\mathbf{x}_i) Y_{k'm'}(\mathbf{x}_j) \\ &\quad \times \langle Y_{km}(\mathbf{x}) (-\Delta_{\mathbb{S}^{d-1}})^n Y_{k'm'}(\mathbf{x}) \rangle \\ &= \sum_{kij} \lambda_k^2 k^n (k+d-2)^n N(d, k) \alpha_i \alpha_j Q_k(\mathbf{x}_i^\top \mathbf{x}_j) \\ &\leq Cp^2 (\alpha^*)^2 \sum_k \lambda_k^2 k^n (k+d-2)^n N(d, k)^2, \end{aligned} \quad (\text{SI.70})$$

where $\alpha^* = \max_j |\alpha_j|$ and $|Q_k(z)| \leq CN(d, k)$ for a universal constant C . A sufficient condition for this sum to converge is that $\lambda_k^2 k^n (k+d-2)^n N(d, k)^2 \sim \mathcal{O}(k^{-1})$ which is equivalent to demanding $\lambda_k N(d, k) \sim \mathcal{O}(k^{-n-1/2})$ since $(k+d-2)^n \sim k^n$ as $k \rightarrow \infty$. \square

9. Spectral Dependence of Learning Curves

We want to calculate how different mode errors change as we add one more sample. We study:

$$\frac{1}{2} \frac{d}{dp} \log \frac{E_\rho}{E_\gamma}, \quad (\text{SI.71})$$

where E_ρ is given by eq. (21). Evaluating the derivative, we find:

$$\begin{aligned} &\frac{1}{2} \frac{d}{dp} \log \left(\frac{E_\rho}{E_\gamma} \right) \\ &= - \left(\frac{1}{\frac{1}{\lambda_\rho} + \frac{p}{\lambda+t}} - \frac{1}{\frac{1}{\lambda_\gamma} + \frac{p}{\lambda+t}} \right) \frac{\partial}{\partial p} \left(\frac{p}{\lambda+t} \right) \end{aligned} \quad (\text{SI.72})$$

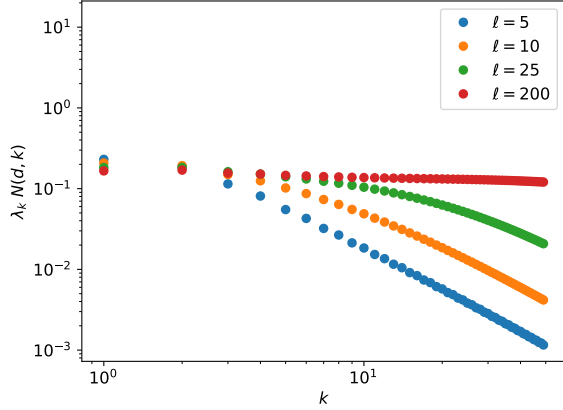


Figure SI.1. Spectrum of fully connected ReLU NTK without bias for varying depth ℓ . As the depth increases, the spectrum whitens, causing derivatives of lower order to have infinite variance. As $\ell \rightarrow \infty$, $\lambda_k N(d, k) \sim 1$ implying that the kernel becomes a Delta function possibly added to a scalar $K(\mathbf{x}, \mathbf{x}') \sim a\delta(\mathbf{x} - \mathbf{x}') + b$ for some constants a and b .

Using eq. (22),

$$\begin{aligned} \frac{\partial t}{\partial p} &= -\frac{\partial}{\partial p} \left(\frac{p}{\lambda+t} \right) \sum_\rho \left(\frac{1}{\lambda_\gamma} + \frac{p}{\lambda+t} \right)^{-2} \\ &= -\gamma \frac{\partial}{\partial p} \left(\frac{p}{\lambda+t} \right), \end{aligned} \quad (\text{SI.73})$$

where we identified the sum with γ . Inserting this, we obtain:

$$\frac{1}{2} \frac{d}{dp} \log \left(\frac{E_\rho}{E_\gamma} \right) = \left[\frac{1}{\frac{1}{\lambda_\rho} + \frac{p}{\lambda+t}} - \frac{1}{\frac{1}{\lambda_\gamma} + \frac{p}{\lambda+t}} \right] \frac{1}{\gamma} \frac{\partial t}{\partial p}. \quad (\text{SI.74})$$

Finally, solving for $\partial t / \partial p$ from (SI.73), we get:

$$\frac{\partial t}{\partial p} = -\frac{1}{\lambda+t} \frac{(\lambda+t)^2 \gamma}{(\lambda+t)^2 - p\gamma} = -\frac{1}{\lambda+t} \text{Tr}(\mathbf{G}^2), \quad (\text{SI.75})$$

proving that $\partial t / \partial p < 0$. Taking $\lambda_\gamma > \lambda_\rho$ without loss of generality, it follows that

$$\frac{d}{dp} \log \left(\frac{E_\rho}{E_\gamma} \right) > 0 \Rightarrow \frac{d}{dp} \log E_\rho > \frac{d}{dp} \log E_\gamma. \quad (\text{SI.76})$$

10. Frequency Dependence of Learning Curves in $d \rightarrow \infty$ Limit

Here, we consider an informative limit where the number of input data dimension, d , goes to infinity.

Denoting the index $\rho = (k, m)$, we can write mode error (SI.35), after some rearranging, as:

$$E_{km} = \frac{(\lambda + t)^2}{1 - \frac{p\gamma}{(\lambda+t)^2}} \frac{\lambda_k \langle \bar{w}_{km}^2 \rangle}{(\lambda + t + p\lambda_k)^2}, \quad (\text{SI.77})$$

where t and γ , after performing the sum over degenerate indices, are:

$$\begin{aligned} t &= \sum_m \frac{N(d, m)(\lambda + t)\lambda_m}{\lambda + t + p\lambda_m}, \\ \gamma &= \sum_m \frac{N(d, m)(\lambda + t)^2 \lambda_m^2}{(\lambda + t + p\lambda_m)^2}. \end{aligned} \quad (\text{SI.78})$$

In the limit $d \rightarrow \infty$, the degeneracy factor (SI.57) approaches to $N(d, k) \sim \mathcal{O}(d^k)$. We note that for dot-product kernels λ_k scales with d as $\lambda_k \sim d^{-k}$ (Smola et al., 2001) (Figure 1), which leads us to define the $\mathcal{O}(1)$ parameter $\bar{\lambda}_k = d^k \lambda_k$. Plugging these in, we get:

$$\begin{aligned} E_{km}(g_k) &= \frac{d^{-k}(t + \lambda)^2}{1 - \tilde{\gamma}} \frac{\bar{\lambda}_k \langle \bar{w}_{km}^2 \rangle}{(t + \lambda + g_k \bar{\lambda}_k)^2} \\ t &= \sum_m \frac{(t + \lambda) \bar{\lambda}_m}{t + \lambda + g_m \bar{\lambda}_m}, \\ \tilde{\gamma} &= \sum_m \frac{g_m \bar{\lambda}_m^2}{(t + \lambda + g_m \bar{\lambda}_m)^2}, \end{aligned} \quad (\text{SI.79})$$

where $g_k = p/d^k$ is the ratio of sample size to the degeneracy. Furthermore, we want to calculate the ratio $E_{km}(p)/E_{km}(0)$ to probe how much the mode errors move from their initial value:

$$\frac{E_{km}(p)}{E_{km}(0)} = \frac{1}{1 - \tilde{\gamma}} \frac{1}{\left(1 + \frac{g_k \bar{\lambda}_k}{t + \lambda}\right)^2} \quad (\text{SI.80})$$

Let us consider an integer l such that the scaling $P = \alpha d^l$ holds. This leads to three different asymptotic behavior of g_k s:

$$\begin{aligned} g_k &\sim \mathcal{O}(d^{l-k}) \gg \mathcal{O}(1), & k < l \\ g_k &= \alpha \sim \mathcal{O}(1), & k = l \\ g_k &\sim \mathcal{O}(d^{l-k}) \ll \mathcal{O}(1), & k > l \end{aligned} \quad (\text{SI.81})$$

If we assume $t \sim \mathcal{O}(1)$, we get an asymptotically consistent set of equations:

$$\begin{aligned} t &\approx \sum_{m>l} \bar{\lambda}_m + a(\alpha, t, \lambda, \bar{\lambda}_l) \sim \mathcal{O}(1), \\ \tilde{\gamma} &\approx b(\alpha, t, \lambda, \bar{\lambda}_l) \sim \mathcal{O}(1), \end{aligned} \quad (\text{SI.82})$$

where a and b are the l^{th} terms in the sums in t and $\tilde{\gamma}$, respectively, and are given by:

$$\begin{aligned} a(\alpha, t, \lambda, \bar{\lambda}_l) &= \frac{(t + \lambda) \bar{\lambda}_l}{t + \lambda + \alpha \bar{\lambda}_l}, \\ b(\alpha, t, \lambda, \bar{\lambda}_l) &= \frac{\alpha \bar{\lambda}_l^2}{(t + \lambda + \alpha \bar{\lambda}_l)^2} \end{aligned} \quad (\text{SI.83})$$

Then using (SI.80), (SI.81) and (SI.82), we find the errors associated to different modes as:

$$\begin{aligned} k < l, & \quad \frac{E_{km}(\alpha)}{E_{km}(0)} \sim \mathcal{O}(d^{2(k-l)}) \approx 0 \\ k > l, & \quad \frac{E_{km}(\alpha)}{E_{km}(0)} \approx \frac{1}{1 - \tilde{\gamma}(\alpha)} \\ k = l, & \quad \frac{E_{km}(\alpha)}{E_{km}(0)} = s(\alpha) \sim \mathcal{O}(1), \end{aligned} \quad (\text{SI.84})$$

where $s(\alpha)$ is given by:

$$s(\alpha) = \frac{1}{1 - \tilde{\gamma}(\alpha)} \frac{1}{\left(1 + \alpha \frac{\bar{\lambda}_l}{t + \lambda}\right)^2}. \quad (\text{SI.85})$$

Note that $\lim_{\alpha \rightarrow 0} \tilde{\gamma}(\alpha) = \lim_{\alpha \rightarrow \infty} \tilde{\gamma}(\alpha) = 0$ and non-zero in between. Then, for large α , in the limit we are considering

$$\begin{aligned} k < l, & \quad \frac{E_{km}(\alpha)}{E_{km}(0)} \approx 0 \\ k > l, & \quad \frac{E_{km}(\alpha)}{E_{km}(0)} \approx 1 \\ k = l, & \quad \frac{E_{km}(\alpha)}{E_{km}(0)} \approx \frac{(\lambda + \sum_{m>l} \bar{\lambda}_m)^2}{\bar{\lambda}_l^2} \frac{1}{\alpha^2}. \end{aligned} \quad (\text{SI.86})$$

11. Decomposition of Risk for Numerical Experiments

As we describe in Section 4.1 of the main text, the teacher functions for the kernel regression experiments are chosen as

$$f^*(\mathbf{x}) = \sum_{i=1}^{p'} \bar{\alpha}_i K(\mathbf{x}, \bar{\mathbf{x}}_i), \quad (\text{SI.87})$$

where the coefficients $\bar{\alpha}_i \sim \mathcal{B}(1/2)$ are randomly sampled from a centered Bernoulli distribution on $\{\pm 1\}$ and the points $\bar{\mathbf{x}}_i \sim p(\mathbf{x})$ are drawn from the same distribution as the training data. In general p' is not the same as the number of samples p . Choosing a function of this form is very convenient for producing theoretical predictions of mode errors as we discuss below.

11.1. Theoretical Mode Errors

Since the matrix elements $\langle \mathbf{G}_{\rho\rho}^2 \rangle$ are determined completely by the kernel eigenvalues $\{\lambda_\rho\}$, it suffices to calculate the

diagonal elements of \mathbf{D} to find the generalization error. For the teacher function sampled in the way described above, there is a convenient expression for $\mathbf{D}_{\rho\rho}$.

The teacher function admits an expansion in the basis of kernel eigenfunctions

$$f^*(\mathbf{x}) = \sum_{\rho} \bar{w}_{\rho} \psi_{\rho}(\mathbf{x}). \quad (\text{SI.88})$$

Using the Mercer decomposition of the kernel we can identify the coefficients

$$f^*(\mathbf{x}) = \sum_{i=1}^{p'} \bar{\alpha}_i K(\mathbf{x}, \bar{\mathbf{x}}_i) = \sum_{\rho} \left(\sum_i \bar{\alpha}_i \psi_{\rho}(\bar{\mathbf{x}}_i) \right) \psi_{\rho}(\mathbf{x}) \quad (\text{SI.89})$$

Comparing each term in these two expressions, we identify the coefficient of the ρ -th eigenfunction

$$\bar{w}_{\rho} = \sum_i \bar{\alpha}_i \psi_{\rho}(\bar{\mathbf{x}}_i). \quad (\text{SI.90})$$

We now need to compute the $D_{\rho\rho}$, by averaging \bar{w}_{ρ}^2 over all possible teachers

$$\begin{aligned} D_{\rho\rho} &= \frac{1}{\lambda_{\rho}} \langle \bar{w}_{\rho}^2 \rangle = \frac{1}{\lambda_{\rho}} \sum_{ij} \langle \alpha_i \alpha_j \rangle \langle \psi_{\rho}(\bar{\mathbf{x}}_i) \psi_{\rho}(\bar{\mathbf{x}}_j) \rangle \\ &= \frac{1}{\lambda_{\rho}} \sum_i \langle \psi_{\rho}(\bar{\mathbf{x}}_i) \psi_{\rho}(\bar{\mathbf{x}}_i) \rangle = \frac{p' \lambda_{\rho}}{\lambda_{\rho}} = p', \end{aligned} \quad (\text{SI.91})$$

since $\langle \psi_{\rho}(\mathbf{x}) \psi_{\rho}(\mathbf{x}) \rangle = \lambda_{\rho}$.

Thus it suffices to calculate $\frac{\partial}{\partial v} g_{\rho}(p, v)$ for each mode and then compute mode errors with

$$E_{\rho} = -d_{\rho} \frac{\partial g_{\rho}(p, v)}{\partial v} \Big|_{v=0} \quad (\text{SI.92})$$

where $\frac{\partial g_{\rho}}{\partial v} \Big|_{v=0}$ is evaluated in terms of the numerical solution for $t(p, 0)$.

11.2. Empirical Mode Errors

By the representer theorem, we may represent the student function as $f(\mathbf{x}) = \sum_{i=1}^P \alpha_i K(\mathbf{x}, \mathbf{x}_i)$. Then, the general-

ization error is given by

$$\begin{aligned} E_g &= \langle (f(x) - f^*(x))^2 \rangle \\ &= \sum_{\rho\gamma} \lambda_{\rho} \lambda_{\gamma} \left(\sum_{j=1}^P \alpha_j \phi_{\rho}(x_j) - \sum_{i=1}^{P'} \bar{\alpha}_i \phi_{\rho}(\bar{x}_i) \right) \\ &\quad \left(\sum_{j=1}^P \alpha_j \phi_{\gamma}(x_j) - \sum_{i=1}^{P'} \bar{\alpha}_i \phi_{\gamma}(\bar{x}_i) \right) \langle \phi_{\rho}(x) \phi_{\gamma}(x) \rangle \\ &= \sum_{\rho} \lambda_{\rho}^2 \left(\sum_{j,j'} \alpha_j \alpha_{j'} \phi_{\rho}(x_j) \phi_{\rho}(x_{j'}) \right. \\ &\quad \left. - 2 \sum_{i,j} \alpha_j \bar{\alpha}_i \phi_{\rho}(x_j) \phi_{\rho}(\bar{x}_i) + \sum_{i,i'} \bar{\alpha}_i \bar{\alpha}_{i'} \phi_{\rho}(\bar{x}_i) \phi_{\rho}(\bar{x}_{i'}) \right). \end{aligned} \quad (\text{SI.93})$$

On the d -sphere, by defining $E_k = \sum_{m=1}^{N(d,k)} E_{km}$ we arrive at the formula

$$\begin{aligned} E_k &= \lambda_k^2 N(d, k) \left(\boldsymbol{\alpha}^{\top} Q_k(\mathbf{X}^T \mathbf{X}) \boldsymbol{\alpha} - 2 \boldsymbol{\alpha}^{\top} Q_k(\mathbf{X}^T \bar{\mathbf{X}}) \bar{\boldsymbol{\alpha}} \right. \\ &\quad \left. + \bar{\boldsymbol{\alpha}}^{\top} Q_k(\bar{\mathbf{X}}^T \bar{\mathbf{X}}) \bar{\boldsymbol{\alpha}} \right). \end{aligned} \quad (\text{SI.94})$$

We randomly sample the $\bar{\alpha}$ variables for the teacher and fit $\alpha = (\mathbf{K} + \lambda \mathbf{I})^{-1} \mathbf{y}$ to the training data. Once these coefficients are known, we can obtain empirical mode errors.

12. Neural Network Experiments

For the “pure mode” experiments with neural networks, the target function was

$$\begin{aligned} f^*(\mathbf{x}) &= \sum_{i=1}^{P'} \bar{\alpha}_i Q_k(\mathbf{x}^{\top} \bar{\mathbf{x}}_i) \\ &= \sum_{m=1}^{N(d,k)} \left(\sum_{i=1}^{P'} \bar{\alpha}_i Y_{km}(\bar{\mathbf{x}}_i) \right) Y_{km}(\mathbf{x}), \end{aligned} \quad (\text{SI.95})$$

whereas, for the composite experiment, the teacher function was a randomly sampled two layer neural network with ReLU activations

$$f^*(\mathbf{x}) = \bar{\mathbf{r}}^{\top} \sigma(\bar{\boldsymbol{\Theta}} \mathbf{x}). \quad (\text{SI.96})$$

This teacher model is a special case of eq. (SI.89) so the same technology can be used to compute the theoretical learning curves. We can use a similar trick as that shown in equation (SI.91) to determine \bar{w}_{ρ} for the NN teacher experiment. Let the Gegenbauer polynomial expansion of $\sigma(z)$ be $\sigma(z) = \sum_{k=0}^{\infty} a_k N(d, k) Q_k(z)$ then the mode error for mode k is $E_k = \frac{a_k^2}{\lambda_k^2} \langle g_k^2 \rangle$ where $\langle g_k^2 \rangle$ is computed with equation (SI.35).

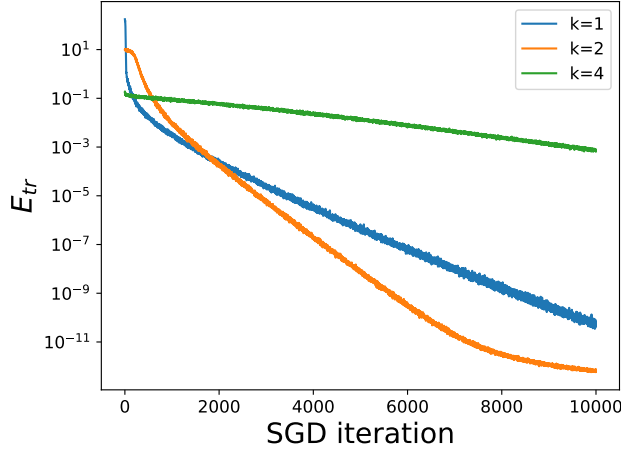
A sample of some training error and generalization errors from pure mode experiments are provided below in Figures [SI.2](#) and [SI.3](#).

12.1. Hyperparameters

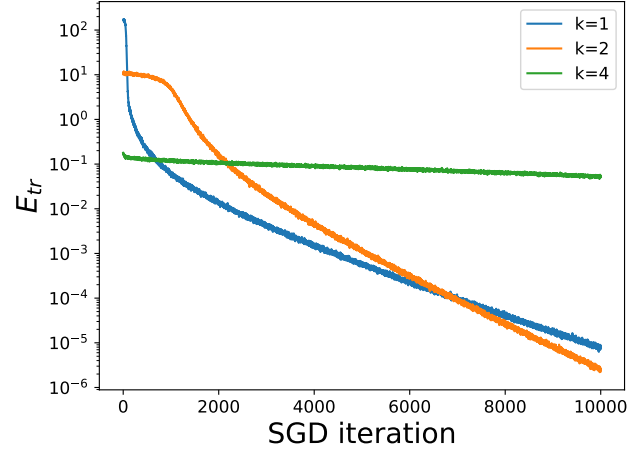
The choice of the number of hidden units N was based primarily on computational considerations. For two layer neural networks, the total number of parameters scales linearly with N , so to approach the overparameterized regime, we aimed to have $N \approx 10p_{max}$ where p_{max} is the largest sample size used in our experiment. For $p_{max} = 500$, we chose $N = 4000, 10000$.

For the three and four layer networks, the number of parameters scales quadratically with N , making simulations with $N > 10^3$ computationally expensive. We chose N to give comparable training time for the 2 layer case which corresponded to $N = 500$ after experimenting with $\{100, 250, 500, 1000, 5000\}$.

We found that the learning rate needed to be quite large for the training loss to be reduced to $\approx 10^{-6}$ of its initial value. For the 2 layer networks, we tried learning rates $\{10^{-3}, 10^{-2}, 1, 10, 32\}$ and found that a learning rate of 32 gave the lowest training error. For the three and four layer networks, we found that lower learning rates worked better and used learning rates in the range from $[0.5, 3]$.



(a) 3 Layer Training Loss; lr = 2



(b) 4 Layer Training Loss; lr = 0.5

Figure SI.2. Training error for different pure mode target functions on neural networks with 500 hidden units per hidden layer on a sample of size $p = 500$. Generally, we find that the low frequency modes have an initial rapid reduction in the training error but the higher frequencies $k \geq 4$ are trained at a slower rate.

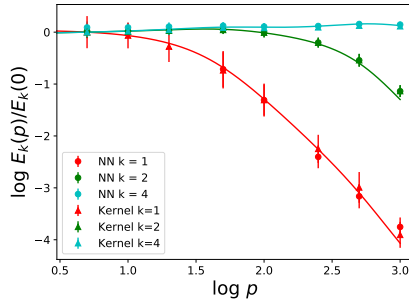
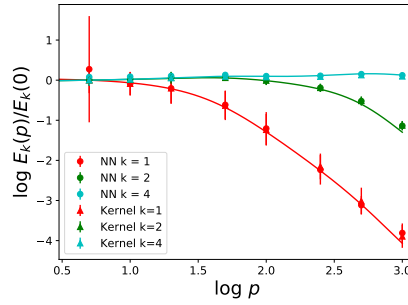
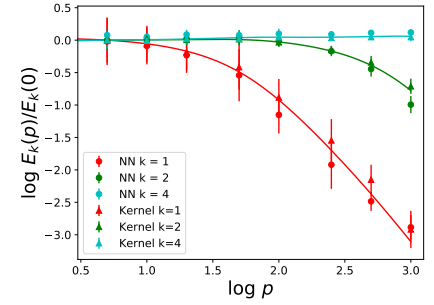
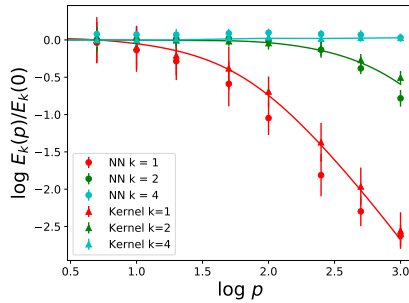
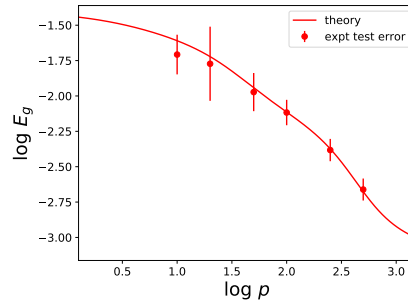
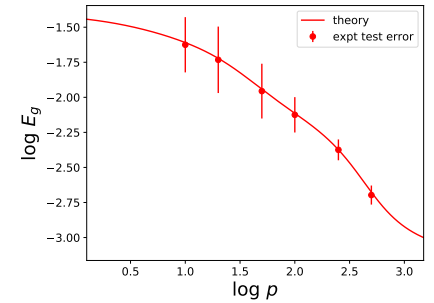

 (a) 2 layer NN $N = 4000$

 (b) 2 layer NN $N = 10^4$

 (c) 3 layer $N = 500$

 (d) 4 layer $N = 500$

 (e) 2 Layer NN Student-Teacher; $N = 2000$

 (f) 2 Layer NN Student-Teacher; $N = 8000$

Figure SI.3. Learning curves for neural networks on “pure modes” and on student teacher experiments. The theory curves shown as solid lines. For the pure mode experiments, the test error for the finite width neural networks and NTK are shown with dots and triangles respectively. Logarithms are evaluated with base 10.